SIMULATION OF FISCHER-TROPSCH FIXED-BED REACTOR IN DIFFERENT REACTION MEDIA

A Thesis

by

LAIAL AHMAD I BANI NASSR

Submitted to the Office of Graduate and Professional Studies of
Texas A&M University
in partial fulfillment of the requirements for the degree of

MASTER OF SCIENCE

Chair of Committee,	Nimir Elbashir
Co-Chair of Committee,	Bukur Dragomir
Committee Member,	Khalid Qaraqe
Head of Department,	Nazmul Karim

December 2013

Major Subject: Chemical Engineering

ABSTRACT

The continuous increase in the global demand for a cleaner energy source has instigated much interest in converting natural gas to ultra-clean fuels and value-added chemicals. Fischer-Tropsch synthesis (FTS) is a key technology for converting syngas, produced from coal, biomass or natural gas, into a variety of hydrocarbon products. Although this technology has been around for decades, commercial development remains relatively slow and limited to use of few reactor configurations (e.g. fixed-bed reactor and slurry-bubble column reactor).

On the lab-scale, supercritical solvents were utilized in FTS as a reaction media since they have the advantages of both the gas-phase reaction (fixed-bed reactor) and the liquid-phase reaction (slurry-bubble column reactor), while simultaneously overcoming their limitations. This work focuses on modeling the behavior in the reactor bed ('macro-scale' assessment) and then zooming into the catalyst pellet itself ('micro-scale' assessment).

The aim of this research is to simulate the heat and mass transfer behavior inside the reactor bed, identify typical conditions that look at the existence and absence of both mass and heat transfer limitations, and to quantify the role of the main controlling parameters on the overall behavior of the reactor bed and on the catalyst effectiveness factor. An often used mathematical model of the fixed-bed reactor was applied to simulate the concentration and temperature profile simultaneously based on the appropriate mass and heat balances at both scales. A second-order ordinary differential

equation was used for a spherical pellet in the radial coordinate for both mass and heat balances, while a one-dimensional steady state pseudo heterogeneous model was used for the reactor bed modeling in the axial direction. In addition, in both models the mass balance equation was expressed in terms of fugacity to account for the non-ideal behavior of the reaction mixture in the SCF-FTS. The thermodynamic properties of the mixture were estimated using the Soave-Redlich-Kwong equation of state (SRK-EOS).

The simulation results of this study showed a high temperature rise in the gas-phase FTS relative to that in the SCF-FTS under a comparable reaction conditions. Carbon monoxide conversion was considerably higher in the SCF compared to the gas-phase reaction. The effect of the particle size on the overall catalyst effectiveness factor was also investigated in both reaction media.

DEDICATION

To my parents and my family

ACKNOWLEDGEMENTS

I would like to thank my committee chair, Dr. Nimir Elbashir, my committee Co-chair, Dr. Bukur Dragomir, my committee member, Dr.Khalid Qaraqe, and Prof. Marcelo Castier, for their guidance and support throughout this research project.

Thanks also go to Dr. Nimir Elbashir's research team, Jan Blank, Rehan Hussain and Elfatih Elmalik, for their continuous help and support in modeling activities.

I also want to extend my thanks to friends, colleagues and faculty and staff for making my time at Texas A&M University at Qatar a unique experience.

Finally, special thanks must be given to my family for their encouragement and support throughout the years.

NOMENCLATURE

i	Species in the reaction mixture
λ^{e}	Pellet effective thermal conductivity
ΔH_r	Heat of reaction
D_i^e	Effective diffusivity of i in catalyst pore
D_{12}	Binary diffusion coefficient, 1 refers to solvent and 2 refers to solute
$D_{i,wax}$	Binary diffusion coefficient of reactants in heavy wax
ρ_{cat}	Catalyst density
T	Temperature
P	Pressure
r	Radius of the pellet
r_i	Rate of formation of compound i
R	Universal gas constant
$R_{cat.}$	Catalyst pellet radius
T^s	Temperature at the pellet surface
T^b	Temperature at the bulk fluid
C_i^s	Reactants concentration at the pellet surface
C_i^b	Reactants concentration at the bulk fluid
f_i^s	Reactant concentration at the pellet surface

f_i^b	Reactant concentration at the bulk fluid
U_s	Superficial fluid velocity
ρ_B	Bulk density of the catalyst per unit volume
λ_L	Thermal dispersion coefficient in the axial direction
U	Overall heat transfer coefficient
d_t	Reactor tube internal diameter
T_{wall}	Wall temperature
M	Molecular weight
V_c	Critical molar volume
P_c	Critical pressure
z_c	Critical compressibility factor
V	Molar volume of the solvent
k	Parameter function of reduced density
ρ_r	Reduced density of the solvent
d_P	Catalyst pore diameter
ε_P	Catalyst porosity
τ	Catalyst tortuosity
f_{CO}	Fugacity of CO
f_{H_2}	Fugacity of H_2
r_{CO}	CO consumption rate

K	Rate constant for the rate of CO consumption ($mol/g_{cat}.min.bar$)
K_1, K_2, K_3	Constants for the rate of CO consumption ($1/bar^{0.5}$,$1/bar^{0.5}$/1/bar)
S	Hexane to syngas ratio (feed)
V	H_2 to CO ratio
k_m	Internal mass transfer coefficient
h	Internal heat transfer coefficient
λ_{Pellet}	Pellet thermal conductivity
λ_{fluid}	Bulk fluid (*n*-Hexane) thermal conductivity
λ_m	Thermal conductivity of the gas mixture at low pressure
λ_m^o	Thermal conductivity of pure gas components at low pressure
Γ	Reduced inverse thermal conductivity
k_m	Thermal conductivity of the gas mixture at high pressure
q	Brokaw parameter
y_1	Mole fraction of light component
y_2	Mole fraction of heavy component
R_e	Dimensionless Reynolds number
S_c	Dimensionless Schmidt number

TABLE OF CONTENTS

LIST OF FIGURES

LIST OF TABLES

1. INTRODUCTION AND LITERATURE REVIEW

1.1 Introduction

With the continuous increase in global demand for cleaner energy sources, Gas-to-liquid (GTL) technology is receiving significant interest as a viable alternative to conventional energy sources. GTL technology is a chemical process that converts natural gas to ultra-clean fuels (i.e. gasoline, jet fuel, diesel and kerosene) and value-added chemicals through what is known as the Fischer-Tropsch synthesis (FTS). Qatar has the third largest natural gas reserves in the world with a total capacity of 910 tcf [1]. This has motivated Qatar to have a long-term vision to establish world-class, commercial-scale GTL facilities. Shell has developed several generations of the FTS fixed-bed reactors that are currently a part of the largest GTL plant in the world, the Pearl GTL Plant in Ras Laffan, Qatar. However, Sasol has developed the slurry-bubble column FTS reactors, which is part of several GTL plants including their Oryx GTL plant in Qatar. These unique large-scale GTL plants lead Qatar to be described as the "world capital of GTL."

Comparing these reactor types, FTS that has been commercially operated using fixed-bed reactors (i.e. gas-phase) provides unique reactant diffusivity and a high rate of reaction. However, the fixed-bed reactor is subjected to local overheating of the catalyst surface that may lead to deactivation of the catalyst active sites and also to favoring light hydrocarbon production (i.e. poor temperature control enhances the termination of growing chains and the methanation reaction route) [2]. Furthermore, the heavy wax

formation inside catalyst pores would limit the accessibility of the reactants (i.e. CO and H_2) to the micropores due to mass transfer and diffusional limitations [3]. The slurry-bubble column reactor is composed of fine catalyst particles suspended in heavy paraffinic slurry at high boiling point. This technology has been developed to overcome the limitation of the gas-phase FTS in fixed-bed reactor as the liquid phase provides an optimum medium for the highly exothermic reaction due to its heat capacity and density [4]. Besides its excellent temperature control, this medium facilitates the *in-situ* extraction of heavy liquid hydrocarbons in addition to other advantages [5, 6]. However, the diffusion of the reactants into the catalyst pores is relatively slow in the slurry- phase FTS such that the overall rate of reaction is considerably lower than that in the gas-phase FTS. Other disadvantages of the slurry-phase FTS are low productivity, low catalyst hold-up, and difficult catalyst separation from the heavy products [3, 7, 8]. Table 1.1 summarizes the main advantages and disadvantages of each reactor type.

Table 1.1: Comparison of advantages and drawbacks for fixed-bed reactor and slurry-bubble reactor [9]

	Fixed-bed reactor	**Slurry-bubble column reactor**
Temperature control	-	+
Product-catalyst separation	+	-
Pressure drop	-	+
Catalyst make-up	-	+
Scale-up	+	-

The previous challenges of the commercial FTS reactors directed research efforts towards the application of a reaction media that provided the advantages of both the gas-phase (i.e., fixed-bed reactor) and the liquid-phase (i.e., slurry-bubble column reactor) while at the same time overcoming their limitations. More importantly, this technology was developed to mitigate the weaknesses of the gas-phase FTS and, at the same time, allow the use of fixed-bed reactor. The supercritical fluid solvents have been suggested as suitable media for FTS due to the desirable advantage of the existing gas-phase transport properties and the liquid-phase heat capacity and solubility while sustaining a single-phase operation where mass transfer barrier is eliminated [10, 11].

1.2 Background

1.2.1 Fischer-Tropsch Synthesis (FTS)

FTS is a well-known catalytic process that converts synthesis gas (i.e., a mixture of carbon monoxide and hydrogen) to ultra-clean fuels and value-added chemicals. FTS was first discovered by Franz Fischer and Hans Tropsch in the 1920s [12] to convert synthesis gas derived from coal into hydrocarbons of varying chain length.

This process can be extended to include different feedstocks, such as natural gas and biomass. The feedstocks are converted first into synthesis gas through gasification of coal and biomass) or reforming of natural gas to form liquid hydrocarbon with different chain lengths. Then the process is named according to the raw material used: coal-to-liquid (CTL), gas-to-liquid (GTL) and biomass-to-liquid (BTL). The process can be divided into three main steps: (1) synthesis gas production, (2) FTS reaction, and (3) product upgrading (see Figure 1.1).

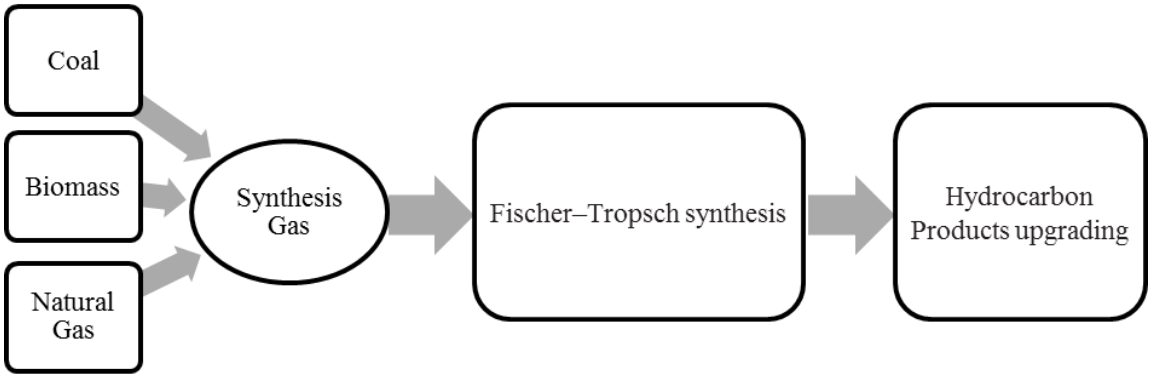

Figure 1.1: Overall schematic for FTS

The fuels produced through FTS are high quality, sulfur- free, aromatics and other contaminants [13]. The product distributions are mainly influenced by syngas feed ratio, temperature, pressure and catalyst type [14]. The most widely used catalysts for this process are cobalt and iron, although other transition metals, such as ruthenium and nickel.

1.2.1.1 Chemistry

The F-T reaction is a polymerization reaction in which the syngas reacts on a catalyst surface, which is usually a cobalt or iron catalyst, to produce paraffins, olefins and oxygenates (i.e. alcohols, aldehydes, acids, and other compounds) [12].

The overall stoichiometry can be described by the following reaction [15]:

$$(2n+1)H_2 + nCO \rightarrow C_nH_{2n+2} + nH_2O \quad -\Delta H = -167\ KJ/mol/CO$$

1.2.1.2 Kinetic and Rate Expressions

Several kinetic studies of the consumption of syngas on Co- and Fe- based catalysts has been reported in the literature (see Table 1.2). Bub and Baerns [16] and Lox

and Froment [17] fitted an empirical power-law rate expression for the reaction rate of carbon monoxide. While Sarup and Wojciechowski [18] and others developed the Langmuir-Hinshelwood-Hougen-Watson (LHHW) rate expression for Co-based catalyst. A detailed literature review of FTS kinetics is given by Van der laan, et al. [19].

Table 1.2: Power-law and LHHW rate expressions for FTS

Rate Expression	Catalyst	Ref.
$-r_{CO} = k\, P_{H_2}^{m}\, P_{CO}^{n}$	Fe	[16, 17]
$-r_{CO} = \dfrac{k P_{CO}^{1/2} P_{H_2}^{1/2}}{\left(1 + k_1 P_{H_2}^{1/2} + k_2 P_{CO}^{1/2} + k_3 P_{CO}\right)^2}$	Co/kieselguhr	[18]
$-r_{CO} = \dfrac{k P_{H_2} P_{CO}}{(1 + k_1 P_{CO})^2}$	Co/MgO/SiO_2	[20]
$-r_{CO} = \dfrac{k P_{H_2}^{1/2} P_{CO}}{\left(1 + k_1 P_{H_2}^{1/2} + k_2 P_{CO}\right)^2}$	Co/kieselguhr	[21]
$-r_{CO+H_2} = \dfrac{k P_{H_2} P_{CO}^{1/2}}{\left(1 + k_1 P_{CO}^{1/2}\right)^3}$	Co/Al_2O_3	[22]

1.2.2 Commercial Scale Fischer-Tropsch Reactors

FTS is an extremely exothermic process, which is an important characteristic that influences the efficiency of the overall system [15]. Consequently, the process development and reactor design was mainly focused on temperature control and effective heat removal [14]. Insufficient heat removal leads to short catalyst lifetime or

catalyst deactivation, low conversion, high methane selectivity and low chain growth probability to produce light hydrocarbon fractions [23, 24].

Currently, three types of FTS reactors are in commercial use: (1) multi-tubular fixed-bed reactor, (2) slurry-bubble column reactor, (3) fluidized-bed reactor (fluidized-bed, circulating or bubbling) (see Figure 1.2). The following sections will provide a brief overview for each reactor type.

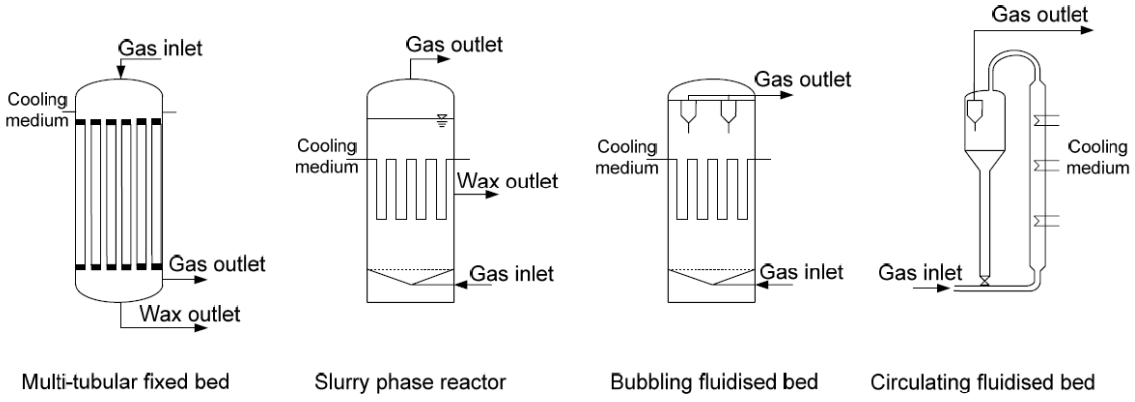

Figure 1.2: Commercial FTS reactors [25]

1.2.2.2 Fixed-Bed Reactor

Fixed-bed reactor was one of the earliest FTS reactors designed. The catalysts are placed into narrow tubes surrounded by cooling water. The syngas is feed through the tubes at high flow rate which creates a turbulent flow. These features ensure rapid heat removal and minimize the rise in temperature. This type of reactor is simple to operate; the separation of liquid products from the catalyst bed is relatively easy. However, the

main disadvantages are the high pressure drop, high capital cost and catalyst make-up is difficult to be replaced during operation. The reactor is used for low- temperature FTS (i.e., operated at a temperature range of 220-250 ºC) to produce long-chain liquid hydrocarbons using a Fe- or CO-based catalyst. Accordingly, three phases are present: gas, liquid and solid [26].

1.2.2.2. Slurry-Bubble Column Reactor

The slurry-bubble column reactor consists of solid catalyst particles suspended in liquid hydrocarbons of high thermal capacity. This reactor type provides an alternative reaction media to overcome some of the limitations of the fixed-bed reactor. The heat generated by the exothermic reaction is absorbed by the bulk flow in the liquid phase FTS reactor, which results in smaller variations in temperature [6, 27]. However, in the slurry-phase the rate of mass transfer of reactants into the catalyst pores is relatively low and, thus, the overall reaction rate is significantly lower than that in the fixed-bed reactor [28]. The main disadvantage of this reactor type is the separation of the liquid products from small catalyst particles..

1.2.2.3 Fluidized-bed Reactor

A fluidized-bed reactor is used for the high-temperature FTS (i.e., operated at temperature range between 320-350 ºC) to produce alkenes or liquid fuels, gasoline and diesel, with a Fe-based catalyst.

1.2.3 Modeling of FTS in a Fixed-Bed Reactor

The simulation of a fixed-bed FTS reactor has been done in several previous studies using different models, such as one- and two- dimensional models. Wang et al.

[29] have used a one-dimensional heterogeneous model to investigate the performance of FTS using fixed-bed reactor. While Jess and Kern [30] developed a two-dimensional pseudo-homogeneous model for FTS in a multi-tubular fixed-bed reactor. The following Table 1.3 shows a summary of related modeling studies that have been published.

Table 1.3: Summary of related modeling studies

Paper Title & Year	Research work & Main Findings	Ref.
Steady State and Dynamic Behavior of Fixed-Bed Catalytic Reactor for Fischer Tropsch Synthesis (1999)	• Simulate the fixed-bed FTS reactor packed with cobalt catalyst using two-dimensional heterogeneous model. • Consider the mass transfer, pore diffusion, momentum, and pressure drop. • Estimate the chemical and physical parameter form experiments or using equation of state.	[31]
Heterogeneous Modeling for Fixed-Bed Fischer Tropsch synthesis Reactor Model and its a Applications (2003)	• Simulate the fixed-bed FTS reactor using one-dimensional heterogeneous reactor model • Study the effect of tube diameter, recycle ratio, cooling temperature and pressure on temperature profile.	[29]
Modeling of Multi-Tubular Reactors for Fischer-Tropsch Synthesis (2009)	• Model of fixed-bed FTS reactor packed with Iron and Cobalt catalst using 1-D & 2-D homogeneous model.	[30]
Fischer-Tropsch Synthesis in a Fixed Bed Reactor (2011)	• Simulate the fixed-bed FTS reactor packed with iron-based catalyst. • Study the effect of different process parameters and operating conditions (i.e. syngas feed ratio, pressure, reactor length) on product distribution.	[32]
A Trickle Fixed-Bed Recycle Reactor Model for the Fischer-Tropsch Synthesis (2012)	• Simulate the trickle fixed-bed FTS reactor using Co- and Fe-based catalyst. • Validate data by SASOL's Arge reactors.	[33]

1.2.4 Supercritical Fluids

Supercritical fluids are substances in a thermodynamic state where their pressure and temperature are higher than the critical pressure (P_C) and temperature (T_C) (see Figure 1.3) [10]. At the supercritical condition, the fluid exists as a single phase having unique physical properties (e.g., diffusivity and heat capacity) that are in between those of the gas and liquid phase [34].

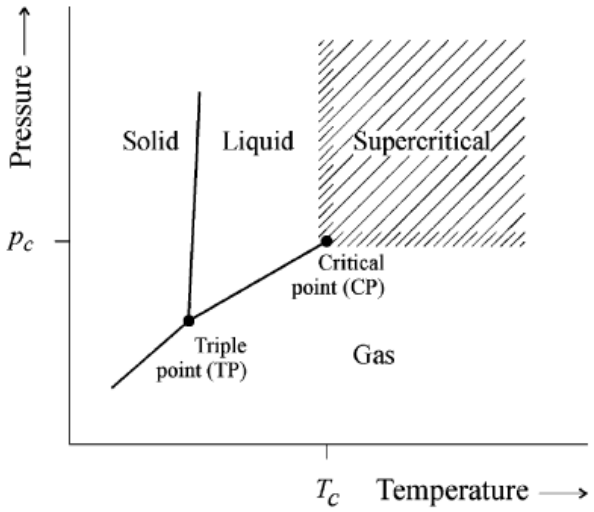

Figure 1.3: Definition of the supercritical state of pure components [35]

Table 1.4 shows the magnitude of supercritical solvents properties compared to the gas and liquid phase. The density of the supercritical fluids is liquid-like, while the viscosity and the diffusivity are more gas-like.

Table 1.4: Magnitudes of physical properties of gases, liquids and supercritical solvents [36]

Physical Quantity	Gas	SCF	Liquid
Density (kg/m^3)	10^0	10^2	10^3
Viscosity (Pa.s)	10^{-5}	10^{-4}	10^{-3}
Diffusivity (m^2/s)	10^{-5}	10^{-7}	10^{-9}-10^{-10}

The utilization of supercritical fluids as media for a chemical reaction provides several advantages for catalytic reactions as shown in the following [34]:

1. Improve the diffusion-control liquid phase reaction by eliminating the gas/liquid and liquid/liquid resistance due to the gas like diffusivity.
2. The reaction environment can be continuously adjusted by a small change in pressure and/or temperature to enhance the reactants and product solubility and to eliminate mass transport resistance.
3. Easy access to the catalyst pores to extract the non- volatile substances due to the low surface tension of SCF.
4. Increase the catalyst lifetime because non-volatile substances can be dissolved in the SCF due to liquid-like density.
5. Enhance the mass transfer because of the high diffusivity and the low viscosity and the heat transfer due to the higher thermal conductivity of SCF than the corresponding gas-phase.

1.2.5 SCF-FTS

A number of papers have attempted to study the reaction performance of the SCF-FTS. Fujimoto, et al. [37], the pioneer of utilizing supercritical solvents in FTS, have investigated the SCF-FTS using *n*-hexane as a solvent. He also compared the reaction performance in the gas phase, liquid phase and SCF using fixed-bed reactor. These efforts were followed by several researchers to study the effect of supercritical solvents on FTS. Table 1.5 provides the main studies published in open literature in the area of SCF-FTS.

Table 1.5: Summary of the main related research work

Paper Title & Year	Operating Condition	Research work & Main Findings	Ref.
Supercritical phase Fischer-Tropsch synthesis (1990)	T = 240°C, P= 45 bar, CO/H_2 = l/2 Solvent/Syngas =3.5 Type of solvent: *n*-Hexane	• The overall rate of the reaction in the supercritical phase reaction was lower than the gas-phase reaction. • The diffusion of the reactants was also lower in the gas-phase compared to the supercritical phase reaction conditions. • Effective removal of heat generated through the exothermic reaction and heavy waxy products from the catalyst pellet in the SCF than that in the gas-phase reaction.	[38]
Supercritical phase Fischer-Tropsch synthesis reaction 3. Extraction capability of supercritical fluids (1991)	T = 240°C, P= 45 bar, CO/H_2 = l/2 Solvent/Syngas =3.5 Type of solvent: *n*-Hexane and *n*-Heptane.	• Heavy wax was effectively extracted from the catalyst bed. • Using *n*-hexane as supercritical solvent gave the highest rate of reaction and highest extraction capability. • High olefin content in the hydrocarbon for SCF reaction.	[12]

Table 1.5: Continued.

Paper Title & Year	Operating Condition	Research work & Main Findings	Ref.
Supercritical Phase Fischer-Tropsch Synthesis: Catalyst Pore-Size Effect (1992)	T = 240°C, P= 45 bar, CO/H_2 = l/2 Solvent/Syngas =3.5 Type of solvent: *n*-Hexane	• For the large pore size, the proportion of the heavy hydrocarbon was high. • While for the small pore size catalyst tended to produce lighter hydrocarbons.	[3]
Enhanced incorporation of ∝-olefins in the Fischer– Tropsch synthesis chain-growth process over an alumina-supported cobalt catalyst in near-critical and supercritical hexane media (2005)	T = (230-260)°C, P= (30-80) bar Type of solvent: *n*-Hexane	• They study the product distribution in the SCF-FTS using cobalt-based catalyst in fixed-bed reactor. • They also measure the critical point of n-Hexane, syngas and products using variable-volume view cell apparatus. • Significant deviation of hydrocarbon distribution from the standard Anderson-Schultz-Flory model.	[15]
Development of a Kinetic Model for Supercritical Fluids Fischer-Tropsch Synthesis (2011)	T = (230 – 250)°C, P= (35-79) bar, CO/H_2 = l/2 Solvent/Syngas =3 Type of solvent: *n*-Hexane	• Derived fugacity-based kinetic models to account for the non-ideal reaction behavior in the gas-phase media and SCF using cobalt-based catalyst.	[24]
Selective Fischer-Tropsch synthesis over an Al_2O_3 Supported cobalt Catalyst in Supercritical Hexane (2003)	T = 250°C, P= (35,41,65 and 80) bar CO/H_2 = l/2 Type of solvent: *n*-Hexane	• The optimum operating conditions to maximize the conversion of carbon monoxide and olefin selectivity are T = 250°C and P=65 bar. • The catalyst bed temperature was well controlled and in SCF-FTS compared to the gas-phase reaction.	[23]

Table 1.5: Continued.

Paper Title & Year	Operating Condition	Research work & Main Findings	Ref.
Effect of Process Conditions on Olefin Selectivity during Conventional and Supercritical Fischer-Tropsch Synthesis (1997)	T = 250°C, P= 55 bar CO/H_2 = l/2 Type of solvent: *n*-Propane	• SCF-FTS is attractive for producing a high molecular weight ∝-olefins. • Total olefin content decreases with increasing syngas molar feed ratio. • Olefin selectivity was independent of reaction temperature. • Total olefin content was greater during SCF-FTS. • High diffusivities and desorption rates of ∝-olefins in the SCF-FTS than the liquid hydrocarbon wax produced in the gas-phase reaction.	[27]
Impact of cobalt-based catalyst characteristics on the performance of conventional gas-phase and supercritical-phase Fischer-Tropsch Synthesis (2005)	T = (230-250)°C, P= (20-65) bar CO/H_2 = l/2 Type of solvent: *n*-Hexane	• SCF-FTS minimize methane selectivity even at high syngas conversions. • While in the gas-phase reaction methane selectivity increases as syngas conversion increases. • The selectivity of CO_2 was lower in the SCF-FTS.	[28]

2. RESEARCH PROBLEM AND OBJECTIVES

2.1 Motivation

The unique properties of the SCF-FTS reaction media, e.g., liquid-like density and heat capacity coupled with gas-like diffusivity, have resulted in many improvements in terms of product selectivity and catalyst activity [23]. However, limited efforts have been devoted to quantify these improvements either with the bulk fluid (i.e., macro scale) or inside confined catalyst pores (i.e., micro scale).

There are several unknowns that need to be addressed to move this technology from lab scale to commercial scale; the following are examples of these questions:

- To what degree could the supercritical fluids media could impact the performance of FTS reactions related to the conventional fixed-bed reactor?
- How will we be able to quantify the role of this media to better understand the in situ behavior of the FTS reactor bed?
- What types of modeling tools could help us to quantify the possible improvements in supercritical fluids FTS?
- Is it possible to model the reactor bed in this non-ideal reaction media while simultaneously investigating the micro and the macro-scale behavior of the reactor bed?
- Will these models provide knowledge about experimentally observed phenomena in SCF-FTS, such as enhancement in the in situ mass and heat transfer processes?

2.2 Objectives

The major objective of this study is to utilize modeling techniques to simulate and predict the performance of a fixed-bed reactor under SCF-FTS reaction condition. To be more specific, the objectives of the present study are:

1. To develop a mathematical model to simulate the concentration and temperature profiles inside the catalyst pellet ("micro-level assessment") under both SCF- and gas-phase FTS.
2. To develop a mathematical model that predicts the heat and mass transfer behavior inside the reactor bed ("macro-level assessment") under the gas-phase and SCF reaction conditions utilizing the catalyst effectiveness factor estimated from micro-level assessment analysis.
3. To investigate the role of the main controlling parameters, such as operating conditions (i.e., pressure and temperature), reaction media (i.e., gas-phase and SCF) and catalyst pellet size.
4. To study the effect of the reaction media and particle size on the overall catalyst effectiveness factor.

3. RESEARCH METHODOLOGY AND APPROACH

The following points summarize the approach used for tackling this research study.

1. Conduct an extensive literature review. The previous section 1.2 provided a summary of the related research work that has already been published on the area of SCF-FTS. The main covered topics were:
    - General descriptions of FTS chemistry, kinetics, reactor types and the advantages and disadvantages of each type.
    - Specifications and modeling techniques for the fixed bed FTS reactor.
    - Background of using SCF in chemical reactions specifically FTS including their advantages.
    - Summarize the operating conditions of the SCF-FTS to include studies on: solvent types, phase behavior, product distribution (ASF distribution), kinetics modeling, selectivity of other products such as CH_4 and CO_2.
2. Develop appropriate governing equations that mainly focus on simulating catalyst particle behavior in gas-phase and SCF-FTS along with appropriate boundary conditions, as described below:
    - Develop models from first principles to simultaneously simulate the internal mass and heat transfer inside the catalyst pellet, which is going to be discussed in Section 4.2.

- Select an appropriate equation of state that best describes the thermodynamic behavior of the system under SCF-FTS reaction conditions.
- Select data and variables (i.e., T, P, CO/H_2, solvent/Syngas, type of solvent and etc.) based on literature review.

3. Construct a set of equations to simulate the reactor bed, as per the following:
   - Develop models to simultaneously simulate the mass, heat and momentum inside the reactor bed (Section 4.3)
   - Identify the interrelated transport and heat transfer parameters and how these parameters are influenced by the reaction conditions (e.g. temperature, pressure, conversion, etc.).
4. Use modeling tools to simulate the mass and heat transfer simultaneously inside the catalyst pellet and the reactor bed.
5. Verify the performance of the simulation models with experimental data and validate the model predictability on generating profiles at different reaction conditions (i.e., pressure temperature, CO conversion, solvent/syngas ratio, etc.).

4. METHODOLOGY: DEVELOPMENT OF REACTOR MODELS

4.1 Introduction

Fixed bed reactor design, construction and operation is one of the most significant costs in building and running any chemical facility. The optimum design and efficient operation of a fixed-bed reactor can be achieved through the use of a modeling tool. Fixed-bed reactor modeling involves a set of mass, heat and momentum balance equations. The models can be validated by comparing the obtained results with experimental data.

The modeling of Fischer-Tropsch fixed-bed reactor is presented in this research project in two scales. Micro-scale modeling, which has been used to simulate the spherical catalyst pellet itself using a second-order, one-dimensional model in the radial direction. The macro-scale modeling has been used to simulate the reactor bed using a one-dimensional steady-state pseudo heterogeneous model (plug-flow model) in the axial direction. The currently used models evaluate the concentration and temperature gradients simultaneously. Moreover, in both models the mass balance equation was derived in terms of fugacity to account for the non-ideal behavior of the reaction media in the SCF-FTS reaction.

The following sections will shows a detailed description of each mathematical model in terms of the main assumptions, conservation equations and numerical method, physico- chemical properties estimation and simulation conditions.

4.2 Micro-Scale Model

In this study, the micro-scale model was developed to simulate the diffusion and reaction in a spherical catalyst pellet (Figure 4.1) under both SCF and gas-phase reaction conditions. The steps involved in modeling a chemical system with diffusion and reaction starts with defining the system and all relevant assumptions, writing mole balance in terms of molar flux on a specific species, using Fick's first law for mass transfer to obtain a second-order differential equation in terms of concentration, stating all relevant assumptions, and then solving the resulting differential equation to obtain the concentration profile. The heat balance equation was also performed in the same manner using Fourier's Law.

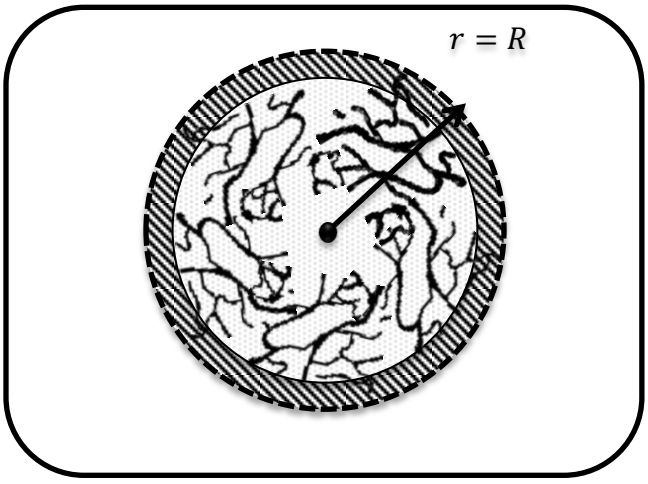

Figure 4.1: Spherical catalyst pellet

4.2.1 Main Assumptions

The Modeling of FTS in a fixed-bed reactor is a complex task, due to the abundant factors to be taken into account in order to obtain a realistic model. The following are the model assumptions:

1. Steady state conditions
2. One-dimensional model in the radial coordinate
3. Spherical Catalyst Pellet with radius R
4. Pores are filled with supercritical *n*-Hexane in the SCF-FTS and heavy wax (*n*-$C_{28}H_{58}$) in the gas phase FTS
5. Single phase operation under SCF reaction condition

4.2.2 Mass and Heat Balances

The mass balance equation for a spherical catalyst pellet assuming steady state conditions, can be expressed by the following second-order differential equation that describes the diffusion and reaction:

$$\frac{D_i^e}{r^2}\frac{d}{dr}\left(r^2\frac{dC_i}{dr}\right) = (-r_i)\rho_{cat.} \qquad \text{Equation 4.1}$$

where i is the species in the reaction mixture, r is the radius of the pellet, r_i is the rate of formation of compound i (mol/g.s), $\rho_{cat.}$is the catalyst density, and D_i^e is the effective diffusivity of i in catalyst pore (cm/s).

The corresponding mass balance for the reactants CO and H_2 are [39]:

$$\frac{D_{CO}^e}{r^2}\frac{d}{dr}\left(r^2\frac{dC_{CO}}{dr}\right) = (-r_{CO})\rho_{cat.} \qquad \text{Equation 4.2}$$

$$\frac{D_{H_2}^e}{r^2}\frac{d}{dr}\left(r^2\frac{dC_{H_2}}{dr}\right) = \left(-r_{H_2}\right)\rho_{cat.} \qquad \text{Equation 4.3}$$

It is important to mention here that the mass balance equation was derived in terms of fugacity to account for the non-ideal reaction mixture in the SCF reaction. The thermodynamic properties of the mixture were calculated using the SRK-EOS. The detailed derivation of Equation 4.1, 4.2 and 4.3 and the derivation in terms of fugacity is given in Appendix A.

The corresponding heat balance equation was derived in the same manner as follows:

$$\frac{\lambda^e}{r^2}\frac{d}{dr}\left(r^2\frac{dT}{dr}\right) = (-r_i)\rho_{cat.}(\Delta H)_r \qquad \text{Equation 4.4}$$

where, i is the species in the reaction mixture, r is the radius of the pellet, r_i is the rate of formation of compound i (mol/g.s), $\rho_{cat.}$ is the catalyst density, λ^e is the pellet effective thermal conductivity (cal/s.cm.k), and ΔH_r is the heat of reaction (cal/mol CO).

4.2.3 Boundary Conditions

Two sets of boundary conditions are considered in the present study [39]:

1. Case (1): Catalyst particles have no external mass transfer limitation, where the concentration at the entrance of the catalyst pore is equal to the concentration in the bulk solution and the concentration remains finite at the center of the catalyst pellet (see Figure 4.2).

$$C_{CO} = C_{CO}^s = C_{CO}^b \qquad at\ r = R_{cat.}$$

$$C_{H_2} = C_{H_2}^s = C_{H_2}^b \qquad at\ r = R_{cat.}$$

$$T = T^s = T^b \qquad at\ r = R_{cat.}$$

$$\frac{dC_{CO}}{dr} = 0 \qquad at\ r = 0$$

$$\frac{dC_{H_2}}{dr} = 0 \qquad at\ r = 0$$

$$\frac{dT}{dr} = 0 \qquad at\ r = 0$$

where, $R_{cat.}$ is the catalyst radius, $C_{CO}^{s}, C_{H_2}^{s} and\ T^{s}$ are the concentrations of CO and H_2 and the temperature at the surface of the catalyst pellet, $C_{CO}^{b}, C_{H_2}^{b} and\ T^{b}$ are the concentrations of CO and H_2 and the temperature at the bulk solution.

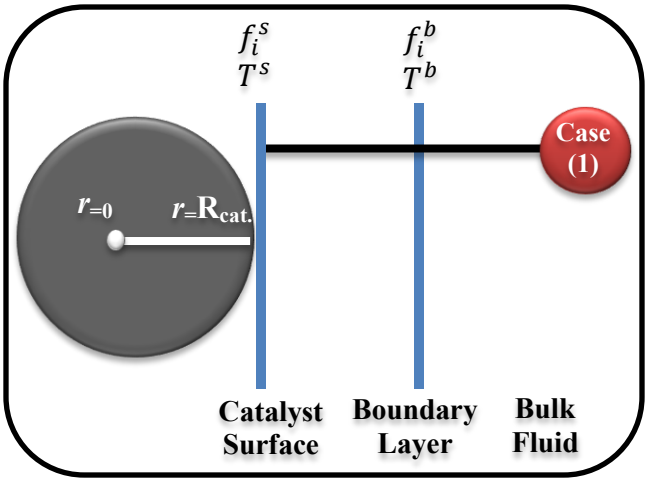

Figure 4.2: Graphical representation of the boundary condition of the system represented in case 1

2. Case (2): Catalyst particles with external mass transfer limitation, where the molar flux to the boundary layer is equal to the convective mass transport across

the boundary layer thickness and the concentration remains finite at the center of the pellet (see Figure 4.3).

$$D_{CO}^{e}\ \frac{dC_{CO}}{dr} = k_m\left(C_{CO}^{b} - C_{CO}^{s}\right) \qquad at\ r = R_{cat.}$$

$$D_{H_2}^{e}\ \frac{dC_{H_2}}{dr} = k_m\left(C_{H_2}^{b} - C_{H_2}^{s}\right) \qquad at\ r = R_{cat.}$$

$$\lambda^{e}\ \frac{dT}{dr} = h(T^{b} - T^{s}) \qquad at\ r = R_{cat.}$$

$$\frac{dC_{CO}}{dr} = 0 \qquad at\ r = 0$$

$$\frac{dC_{H_2}}{dr} = 0 \qquad at\ r = 0$$

$$\frac{dT}{dr} = 0 \qquad at\ r = 0$$

where k_m is the internal mass transfer coefficient and h is the internal heat transfer coefficient. The detailed calculation for k_m and h is given in Appendix B.

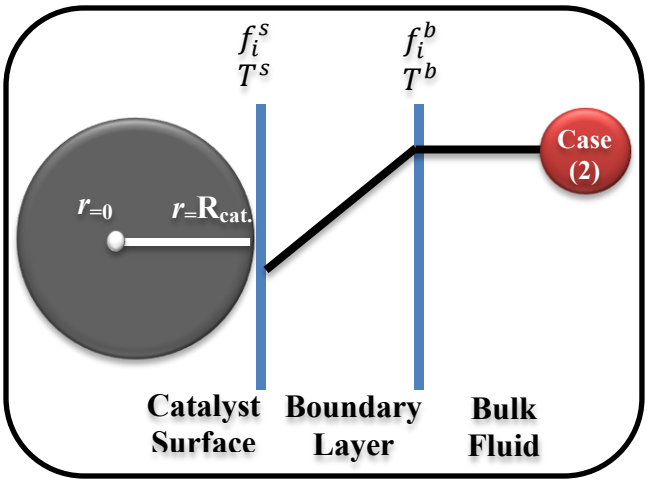

Figure 4.3: Graphical representation of the boundary condition of the system represented in case 2

4.2.4 Kinetics

In the present study, a LHHW kinetic model was used to express the reaction behavior in both the conventional gas-phase FTS and the nonconventional SCF-FTS. The kinetic model was developed from experimental data for an alumina-supported cobalt catalyst (15% Co/Al_2O_3) in a fixed-bed reactor. Also the model was derived in terms of fugacity to account for the non-ideal behavior reaction mixture under high pressure.

$$-r_{CO} = \frac{K f_{CO}^{1/2} f_{H_2}^{1/2}}{\left(1 + K_1 f_{H_2}^{1/2} + K_2 f_{CO}^{1/2} + K_3 f_{CO}\right)^2} \qquad \text{Equation 4.5}$$

where f_{CO} and f_{H_2} are the fugacities of CO and H_2, respectively (bar), r_{CO} is CO consumption rate (mol/g_{cat} min), K, K_1, K_2 and K_3 are the kinetics parameters.

The kinetic parameters for this model were reported by Mogalicherla and Elbahsir [24] at T=513 K for the near critical and SCF-FTS reaction and gas-phase FTS reaction. The following Table 4.1 shows the temperature dependence of the kinetic constants expressed by the Arrhenius equation.

Table 4.1: Kinetic parameters for SCF and gas-phase at T=513 K [24]

Kinetic Parameter	**SCF-FTS**	**Gas Phase FTS**
K(mol/g_{cat}.min.bar)	$4 \times 10^{-4} \exp\left[-12496.99\left(\frac{1}{T}-\frac{1}{315}\right)\right]$	$3 \times 10^{-4} \exp\left[-8960.78\left(\frac{1}{T}-\frac{1}{315}\right)\right]$
K_1 ($bar^{-0.5}$)	$16.9 \times 10^{-2} \exp\left[6025.98\left(\frac{1}{T}-\frac{1}{315}\right)\right]$	$24 \times 10^{-2} \exp\left[7072\left(\frac{1}{T}-\frac{1}{315}\right)\right]$
K_2 ($bar^{-0.5}$)	$20 \times 10^{-2} \exp\left[-17981.77\left(\frac{1}{T}-\frac{1}{315}\right)\right]$	$16 \times 10^{-2} \exp\left[-17007.45\left(\frac{1}{T}-\frac{1}{315}\right)\right]$
K_3 (bar^{-1})	$2 \times 10^{-4} \exp\left[8996.88\left(\frac{1}{T}-\frac{1}{315}\right)\right]$	$1 \times 10^{-4} \exp\left[8995.3\left(\frac{1}{T}-\frac{1}{315}\right)\right]$

4.2.5 Operating Conditions and Catalyst Physical Properties

The operating conditions and catalyst physical properties used for simulation are given in the following Table 4.2.

Table 4.2: Operating conditions and catalyst properties

Temperatures, T	513 K
Total Pressure, P	80 bar
H_2/CO feed ratio, V	2
n-Hexane/Syngas ratio, S	3
Catalyst Type	Co/Al_2O_3
Pellet shape	Spherical
Pellet diameter, d_{Pellet}	1 mm
Pellet porosity, ε_p	0.5
Pellet density, ρ_{cat}	1.5 g/cm^3
Pellet tortuosity,τ	3

4.2.6 Effective Diffusion Parameters

4.2.6.1 For SCF Reaction: Catalyst Pores Filled with Supercritical n-Hexane

Catalyst pores have different cross-sectional areas and the paths are tortuous. It will be hard to describe the diffusion inside each tortuous pathway. Accordingly, the effective diffusivity is used to account for the average diffusion taking place at any position inside the catalyst pellet. The following equation is used to calculate the effective diffusivity using the binary diffusion coefficients, catalyst porosity (which is the volume of the void divided by the total volume), constriction factor (which accounts for a different cross-sectional area) and tortuosity (which is the actual distance the molecule travels divided by the shortest distance) [39]:

$$D_i^e = \frac{D_{21}\,\varepsilon_P\,\sigma_C}{\tau} \qquad \text{Equation 4.6}$$

where D_{21} is the binary diffusion coefficient of solute (2) in solvent (1), ε_P is the catalyst porosity, σ_C is the constriction factor and τ is the catalyst tortuosity.

The ability to predict the binary diffusion coefficients in SCF is considerably important to the design and efficient operation of SCF-FTS. In this research work, binary diffusion coefficients were estimated using the correlation proposed by He [40]. This correlation determines the binary diffusion coefficient of liquid and solid solutes in supercritical solvents, and it was tested for more than 107 solute-solvents systems including *n*-Hexane. The correlation required solvent properties (i.e., critical pressure, critical volume, molecular weight and density), solute properties (i.e., molecular weight) and system temperature as shown below:

$$D_{21} = \left[0.61614 + 3.0902 * \exp\left(-0.87756\frac{\sqrt{M_1 V_{C1}}}{P_{C1}}\right)\right] * 10^{-6}\left(V_1^k - 23\right) * \sqrt{\frac{T}{M_2}} \qquad \text{Equation 4.7}$$

where the subscript 1 and 2 refers to solvent and solute respectively, M is the molecular weight (g/mol), V_C is the critical molar volume (cm^3/mol), P_C is the critical pressure (bar), V is the molar volume of the solvent (cm^3/mol), T is the temperature (K) and the parameter k is a function of solvent reduced density (ρ_r) as the following:

$$k = 1 \qquad for \qquad \rho_r > 1.2$$

$$k = 1 + {(\rho_r - 1.2)}\Big/{\sqrt{M1}} \qquad for \qquad \rho_r < 1.2$$

In is study, the correlation was used to calculate the diffusivity of reactants (CO and H_2) in supercritical *n*-Hexane, which was used as a solvent in several SCF-FTS research studies.

The detailed step-by-step calculation for the effective diffusivity of CO and H_2 in supercritical *n*-Hexane is presented in Appendix C.

4.2.6.2 For Gas phase reaction: Catalyst Pores Filled with Heavy Wax

The effective diffusivity for the gas-phase reaction is calculated in the same manner using Equation 4.7 except for the binary diffusion coefficient. In SCF-FTS reaction, the binary diffusion coefficient was calculated assuming that the reactants diffuse through the solvent (*n*-Hexane), while in the gas-phase FTS reaction; it will be calculated assuming that the reactant diffuses through the heavy wax.

The binary diffusion coefficient for the case when the catalyst pores are filled with liquid wax was calculated using the following correlation proposed by Yong Wang et al. [41]. These correlations assume that the liquid wax is *n*-$C_{28}H_{58}$ and it was simply derived by fitting the reported diffusivity of CO and H_2 is *n*-$C_{28}H_{58}$, as shown below in Equations 4.9 and 4.10:

$$D_{CO,Wax} = 5.584 \times 10^{-7} \exp\left(\frac{-1786.29}{\mathrm{T}}\right) (m^2/\mathrm{s}) \qquad \text{Equation 4.8}$$

$$D_{H_2,Wax} = 1.085 \times 10^{-6} exp\left(\frac{-1624.63}{T}\right) (m^2/s) \qquad \text{Equation 4.9}$$

4.2.7 Effective Thermal Conductivity

4.2.7.1 For SCF Reaction: Catalyst Pores Filled with Supercritical n-Hexane

The effective thermal conductivity of porous catalyst plays a significant role in determining the temperature gradient inside the catalyst pellet, especially for highly exothermic reactions. The following relationship was used to predict an approximation for the effective thermal conductivity as a function of the pellet porosity and the thermal conductivity of both the bulk fluid and the catalyst pellet [42]:

$$\lambda^e = \lambda_{Pellet}\left(\frac{\lambda_{fluid}}{\lambda_{Pellet}}\right)^{\varepsilon_p} \quad \text{Equation 4.10}$$

where λ_{Pellet} is the catalyst pellet thermal conductivity (W/m.K) and λ_{fluid} is the bulk fluid (*n*-Hexane) thermal conductivity (W/m.K).

In this work, the thermal conductivity of catalyst pellet was used based on the correlation developed by Wu, et al. [43]. This correlation was developed for a cobalt-based catalyst for FTS over the temperature range from 160 ˚C to 255 ˚C. Also, it was derived by fitting the catalyst thermal conductivity into a linear relationship with temperature as follows:

$$\lambda_{Pellet} = a + bT \quad (W/m.℃) \quad \text{Equation 4.11}$$

where the constants a and b were calculated by linear regression from the experimental data, a = 0.8652, b = 0.00108.

Equation 4.12 can be rewritten as given bellow:

$$\lambda_{Pellet} = 0.8652 + 0.00108\ (T - 273.15) \quad (W/m.K) \quad \text{Equation 4.12}$$

Calculating the thermal conductivity for the bulk fluid (i.e. *n*-Hexane) at supercritical phase using the available correlation is a complex task [44]. Near the critical point, the liquid solvent behaves somewhat like a dense gas, and the thermal

conductivity varies significantly with a small change in the pressure or temperatures. The thermal conductivity of *n*-Hexane near the critical point can be estimated based on dense gas thermal conductivity correlations developed by Stiel and Thodos as follows [45] (see Appendix D for more details).

In the present research work, the thermal conductivity of *n*-Hexane as a function of temperature was obtained using Aspen Plus® simulation package in the near critical and supercritical region. Aspen Plus® physical properties system was used to calculate *n*-Hexane thermal conductivity utilizing SRK-EOS at different temperature and pressure to fit the following polynomial equation for the sake of simulate on.

$$\lambda_{fluid} = a\left(\frac{P}{65}\right)^{b}\left(\frac{T}{235}\right)^{C} \qquad \text{Equation 4.13}$$

where the parameter a, b and c are constants calculated by linear regression using Aspen data, $a = 0.000142,\ b = 2.017551$ and $c = 0.218024$.

Equation 4.13 can be represented as follows:

$$\lambda_{fluid} = 0.000142\left(\frac{P}{65}\right)^{2.017551}\left(\frac{T}{235}\right)^{0.218024} \qquad \text{Equation 4.14}$$

The data obtained from Aspen Plus® and the detailed calculation to obtain the following expression of *n*-Hexane thermal conductivity at near critical and supercritical phase is shown in Appendix D.

4.2.7.2 For Gas Phase Reaction: Catalyst Pores Filled with Heavy Wax

The effective thermal conductivity for the gas–phase (i.e., reactants: CO, H_2 and inert: N_2) was estimated by two steps [45]:

1. Estimate the thermal conductivity of the gas mixture at low pressure using Stiel and Thodos correlations [45].
2. To account for the influence of high pressure in the system, the thermal conductivity was estimated using Brokaw's empirical method [45].

Stiel and Thodos [45] correlations (Equation 4.15-4.17) are generally used to calculate the thermal conductivity at low pressure knowing the reduced density of the gas mixture.

$$(\lambda_m - \lambda_m^o)\Gamma z_c^5 = 14.0 \times 10^{-8}[\exp(0.535\,\rho_r) - 1] \quad for \quad \rho_r < 0.5 \qquad \text{Equation 4.15}$$

$$(\lambda_m - \lambda_m^o)\Gamma z_c^5 = 13.1 \times 10^{-8}[\exp(0.67\,\rho_r) - 1.069] \quad for\ 0.5 < \rho_r < 2.0 \qquad \text{Equation 4.16}$$

$$(\lambda_m - \lambda_m^o)\Gamma z_c^5 = 2.976 \times 10^{-8}[\exp(1.155\,\rho_r) + 2.016] \quad for\ 2.0 < \rho_r < 2.8 \qquad \text{Equation 4.17}$$

where λ_m is the thermal conductivity of the gas mixture (W/m.K), λ_m^o is the thermal conductivity calculated from pure component thermal conductivity (W/m.K), z_C is critical compressibility factor and Γ is the reduced inverse thermal conductivity $(W/m.K)^{-1}$.

Then, the thermal conductivity for the gas mixture at high pressure assuming two component mixtures (syngas and N_2) was calculated using Brokaw's empirical method [45].

$$k_m = q k_{mL} + (1 - q) k_{mR} \qquad \text{Equation 4.18}$$

$$k_{mL} = y_1\lambda_1 + y_2\lambda_2 \quad and \quad \frac{1}{k_{mR}} = \frac{y_1}{\lambda_1} + \frac{y_2}{\lambda_2} \qquad \text{Equation 4.19}$$

where k_m is the thermal conductivity of the gas mixture at high pressure, q is the Brokaw parameter, y_1 is the mole fraction of the light component, y_2 is the mole fraction

of the heavy component, λ_1 is the thermal conductivity of component 1 (syngas) at low pressure, and λ_2 is the thermal conductivity of component 2 (N_2). The detailed calculation is given in Appendix D.

4.2.8 Effectiveness Factor Calculation

For the catalyst pellet simulation, the overall catalyst effectiveness factor is defined here as the ratio of the actual overall rate of reaction to the rate of reaction if the catalyst surface was exposed to the bulk conditions. The overall effectiveness factor can be calculated using the following equation [39]:

$$\eta = \frac{3}{{R_p}^3} \frac{\int_0^{R_p} r_{CO} r^2 dr}{r_{CO,\ bulk}} \qquad \text{Equation 4.20}$$

4.3 Macro-Scale Model

This section considers the FTS taking place in the backed bed of the catalyst pellets rather than one single pellet (i.e., zooming out from micro-scale to macro-scale) to understand the reactor bed behavior in supercritical phase and gas-phase reaction.

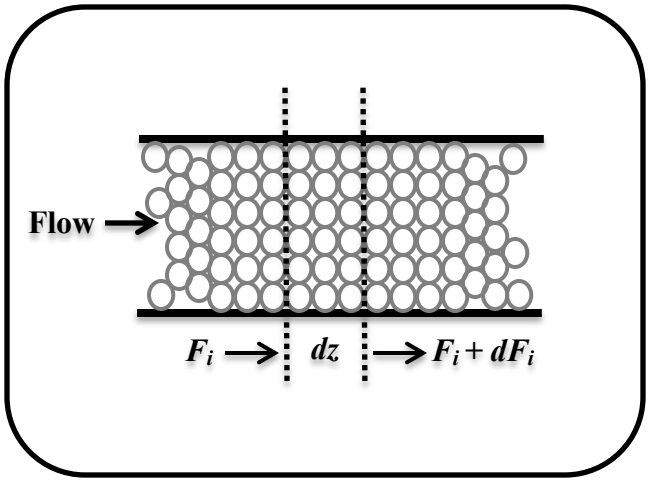

Figure 4.4: Illustrations of fixed-bed reactor

The advantages of the supercritical-phase compared with the gas-phase reaction media have been proved experimentally by many researchers [8, 23, 38]. The purpose of macro-scale modeling is to capture these advantages from the modeling results.

A one-dimensional heterogeneous mathematical model of fixed-bed reactor was developed in this work to obtain the concentration and temperature profiles in the reactor bed (see Figure 4.4). The steps involved in modeling an FTS reactor bed at the macro-scale are the following:

1. Define the system boundaries
2. State all relevant assumptions
3. Write the reactor bed balance equations for mass, heat and momentum and explain their physical significance
4. Define initial conditions and their physical interpretation

5. Calculate all necessary variables to solve the balance equations (e.g., superficial velocity, overall heat transfer coefficient, etc.)
6. Use a modeling tool to solve the balance equations
7. Validate the model outcomes with experimental data published in the literature

4.3.1 Main Assumptions

A number of assumptions were made in order to simplify the complex phenomena of heat, mass and momentum into a mathematical model. The main assumptions are:

1. Steady state conditions.
2. One-dimensional plug-flow model in the axial direction.
3. Constant superficial velocity in the axial direction.
4. Catalyst pores are filled with *n*-Hexane in the SCF-FTS and heavy wax (*n*-$C_{28}H_{58}$) in the gas phase FTS.
5. Single phase operation under SCF reaction condition.

4.3.2 Mass, Heat and Momentum Balances

The mass balance equation of a tube packed with a solid catalyst (system in Figure 4.2) was developed using a one-dimensional steady state model in the axial direction as per the following first-order differential equation:

$$-u\frac{dC_i}{dz} = \eta_o \rho_B (-v_i) r_i \qquad \text{Equation 4.21}$$

where u is the superficial velocity, C_i is the concentration of species i, η_o is the overall effectiveness factor, ρ_B is the bed density (mass of catalyst/volume of bed), v_i is the

stoichiometric coefficient of species i, and r_i is the rate of reaction over the solid catalyst (mole/mass of catalyst/time).

In Equation 4.21, the rate of reaction per unit mass of the catalyst is multiplied by the bed density in order to obtain the rate of reaction per unit volume in the mass balance equation. Additionally, the overall effectiveness factor is used to relate the actual overall rate of reaction within the catalyst pellet to the rate that would result in bulk fluid conditions.

The fugacity-based mass balance was estimated for the previous Equation 4.21 to account for the non-ideal reaction mixture under high pressure condition. The detailed derivation of Equation 4.21 and the fugacity-based mass balance is given in Appendix E.

An energy balance equation was also developed to account for the temperature gradients for the fixed-bed reactor with heat exchange (i.e., heat is either added or removed) in the axial direction. The energy balance for the reactor bed used in this work is shown in equation 4.22 [39, 46].

$$u_s \rho_g C_p \frac{dT}{dz} = (-\Delta H)\eta r_{CO} \rho_B - \frac{4U}{d_t}(T - T_r) \qquad \text{Equation 4.22}$$

To account for the pressure drop through the porous backed bed, a common pressure drop equation was used ('Ergun equation') as per the following [39, 47]:

$$-\frac{dP}{dz} = f \frac{\rho_g {u_s}^2}{d_p} \qquad \text{Equation 4.23}$$

For Equation 4.22, the bed friction factor f was calculated using Hicks's correlation for spherical particles [47] as follows:

$$f = 6.8\frac{\left(1-\varepsilon_p\right)^{1.2}}{\varepsilon_p^3}Re^{-0.2} \qquad \text{Equation 4.24}$$

4.3.3 Initial Conditions

The initial conditions considered in the present study are based on the inlet conditions of the reactor bed entrance ($z = 0$). The inlet conditions used are: (1) the inlet concentration, (2) the inlet temperature and (3) the inlet pressure.

- For mass equation:

$$C_{CO} = C_{CO,o} \qquad at\ z = 0$$

- For heat equation

$$T = T_{in} \qquad at\ z = 0$$

- For momentum equation

$$P = P_{in} \qquad at\ z = 0$$

4.3.4 Kinetics

For the macro-level assessment, the same rate expression was used (see Section 4.2.4) for CO consumption.

4.3.5 Operating Conditions and Fixed- Bed Reactor Properties

The operating conditions and the fixed-bed reactor properties used for simulation are given in the following Table 4.3. Figure 4.5 shows a schematic representation of the lab-scale fixed-bed reactor dimensions used in the simulation.

Table 4.3: Simulation conditions employed in the SCF- and gas-phase FTS

Temperatures, T	513 K
Total Pressure, P	80 bar
Inlet Flow Rate (Std.)	50 cm^3/min
H_2/CO feed ratio	2
n-Hexane/Syngas ratio, S	3
Tube Length	40.64 cm
Bed Length	5 cm
Tube Internal Diameter	1.57 cm
Wall Thickness, d	0.8 cm

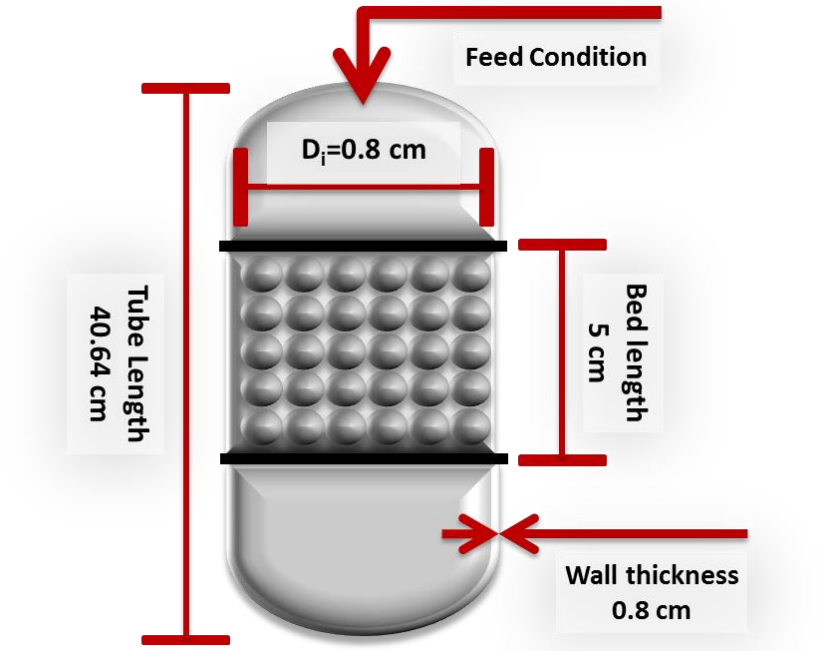

Figure 4.5: Schematic diagram of the lab scale fixed-bed reactor dimensions

4.3.6 Overall Heat Transfer Calculation

The overall heat transfer coefficient in a fixed-bed reactor was estimated using the following equation [47]:

$$\frac{1}{U} = \frac{1}{\alpha_i} + \frac{d}{\lambda_{wall}}\frac{A_b}{A_m} + \frac{1}{\alpha_u}\frac{A_b}{A_u} \qquad \text{Equation 4.25}$$

where α_i is the heat transfer coefficient on the bed side, α_u is the heat transfer medium side, λ_{wall} is the heat conductivity of the wall, A_b is the heat exchanging surface areas on the bed side, A_u is the heat transfer medium side, $A_m$is the log mean of A_b and A_u and d is the reactor tube wall thickness.

The heat transfer coefficient on the bed side can be found using the following correlation proposed by De wasch and Froment [48].

$$\alpha_i = \alpha_i^0 + 0.033\frac{\lambda_g}{d_p}\mathrm{Pr}_g\mathrm{Re}_g \qquad \text{Equation 4.26}$$

$$\alpha_i^0 = \frac{10.21\lambda_e^0}{{d_t}^{4/3}} \qquad \text{Equation 4.27}$$

where α_i^0 and λ_e^0 are the static contribution and the static contribution to the effective thermal conductivity, respectively. The detailed calculation of the overall heat transfer coefficient is presented in Appendix F.

4.4 Numerical Solution: MATLAB Implementation

As was mentioned previously, the aim of this study was to develop an appropriate technique to simultaneously evaluate the mass and heat transfer inside the catalyst pellet and reactor bed itself. This, however, considerably complicates the task of finding a numerical solution. MATLAB is a powerful modeling tool that has the

ability to solve a system of ODE's, either boundary-value problem (BVP) or initial-value problem (IVP). Two different cases were developed for the modeling task. The first case is the micro-level modeling in the form of ordinary differential Equations 4.3, 4.4 and 4.5 together with the boundary conditions, lead to a two point BVP. The resulting systems of heat and mass balance equations were solved simultaneously by utilizing bvp4c function from MATLAB. This case focuses on the concentration and temperature distribution inside the catalyst pellet, in order to study the effect of heat and mass transfer limitations. As a part of the micro-level modeling, the catalyst effectiveness factor was estimated using trapz function that computes an approximation for the integral through the trapezoidal method. While the second case is the macro-scale modeling given by Equations 4.17, 4.18 and 4.19 together with the initial conditions, lead to an IVP. The obtained equations were solved using ode45 function from MATLAB. This case is mainly focusing on the overall behavior of the reactor bed itself. The steps involved in the modeling are as per the following:

1. Define the research problem and develop mathematical model for the system.
2. Formulate the mathematical equation and use mathematical simulator to compute the numerical solution.
3. Use experimental data to verify the numerical results obtained from MATLAB simulator (see Figure 4.6).

A detailed explanation of the developed modeling code located in Appendix G.

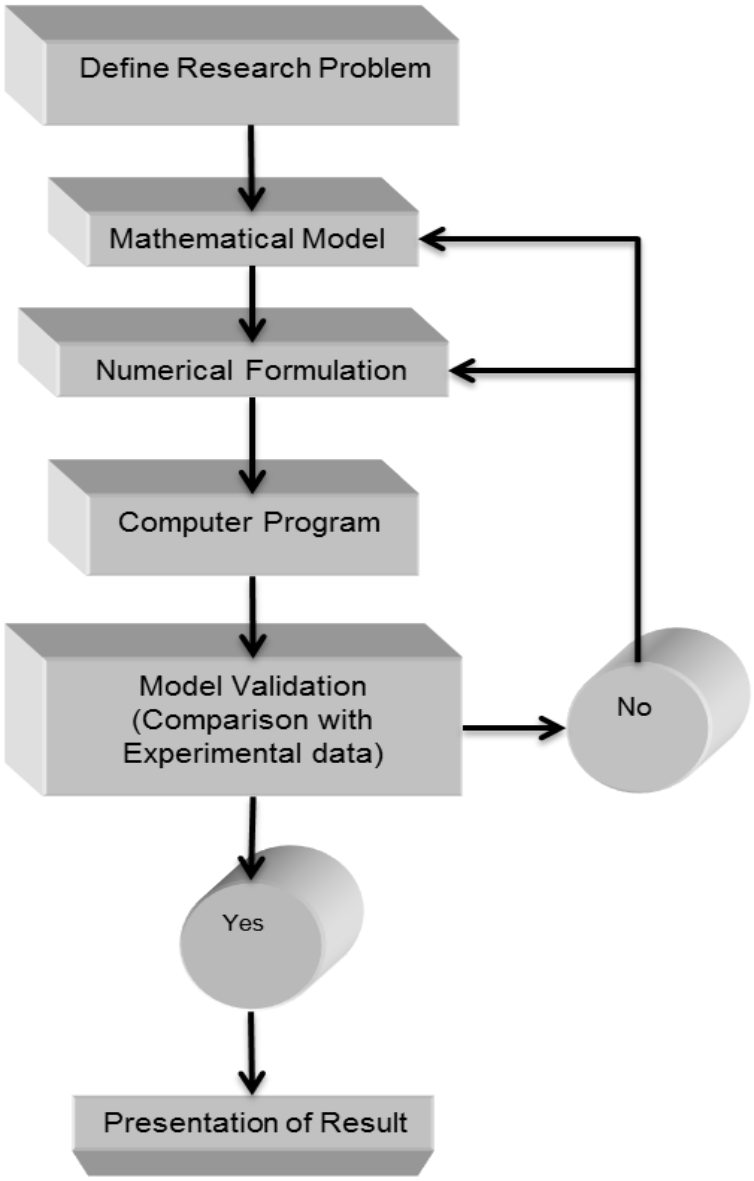

Figure 4.6: Representation of the steps involved in the modeling

5. RESULTS AND DISCUSSION

The following sections present the outcomes of mass, energy and momentum balances conducted in this study. The first section highlights the main results for the micro-scale assessment in terms of the concentration profile, temperature profile and effectiveness factor. It will also investigate the role of the main controlling parameters such as pressure, pellet size and reaction media. While the second section underlines the results of macro-scale assessment that are considered as the principle contribution to the study, showing the impact of supercritical solvents on the temperature profile distribution. This section will also address the impact of the conversion on the overall catalyst effectiveness factor.

5.1 Micro-scale Modeling

5.1.1 Diffusivities of H_2 and CO

The calculated results for the binary diffusion coefficient and the effective diffusivity in the conventional gas-phase FTS reaction and the SCF-FTS reaction are listed in the following Table 5.1. The binary diffusivity of the reactants in the supercritical *n*-Hexane was estimated using Equation 4.8. The diffusivity of CO was found to be four times less than that of the H_2, under the specified reaction conditions. While the binary diffusion coefficient in the heavy hydrocarbons under the gas-phase reaction conditions was obtained using Equation 4.9 and 4.10. According to the results presented in Table 5.1, it is obvious that the diffusivity of the H_2 and CO is much higher in the SCF-FTS compared to the gas-phase FTS. This is due to the complex mixture of

hydrocarbons produced in a typical industrial FTS with fixed-bed reactors. Therefore, the catalyst pores are filled with liquid hydrocarbons, which in turn decrease the reactants accessibility [41, 49]. A similar finding has been reported by Yan et al. [50] at different reaction conditions using *n*-Pentane as a supercritical solvent.

Table 5.1: Binary diffusion coefficient and effective diffusivity

Supercritical phase	Gas phase
$D_{CO-Hexane} = 1.03 \times 10^{-3}\ cm^2/s$	$D_{CO-Wax} = 1.72 \times 10^{-4}\ cm^2/s$
$D_{H_2-Hexane} = 3.86 \times 10^{-3}\ cm^2/s$	$D_{H_2-Wax} = 4.57 \times 10^{-4}\ cm^2/s$
$D^e_{CO-Hexane} = 1.33 \times 10^{-4}\ cm^2/s$	$D^e{}_{CO-Wax} = 2.86 \times 10^{-5}\ cm^2/s$
$D^e_{H_2-Hexane} = 6.43 \times 10^{-4}\ cm^2/s$	$D^e{}_{H_2-Wax} = 7.62 \times 10^{-5}\ cm^2/s$

5.1.2 Concentration Profile

The simulated intra-pellet concentration profiles for the reactants ($CO+H_2$) inside catalyst pellet both in the SCF-FTS and gas-phase FTS are shown in the following Figure 5.1 and 5.2. It is clear from the concentration profiles that the diffusivity of the syngas in the heavy waxy product under conventional gas-phase FTS is much slower than in the SCF-FTS. This leads to the significant profiles inside the catalyst pellet. Yan et al. [50] presented similar findings (see Figure 5.3) using power rate law for F-T kinetics and slightly different reaction conditions. As can be noticed from Figure 5.1, CO concentration drops from 5.94 bar to 3.63 bar as it enters the mouth of the pore

(when r/RP =1). It was also noticed that the catalyst pores are rich with H2 along all the positions (from r/RP =1 to the center of the pellet r/RP =0). This is because of the very high effective diffusivity of H2 relative to CO, even under supercritical condition.

It should be noted here that we simulated the SCF-FTS reactor utilizing experimental data reported in literature for a cobalt-based catalyst under both conventional gas-phase FTS and near critical and supercritical FTS [8].

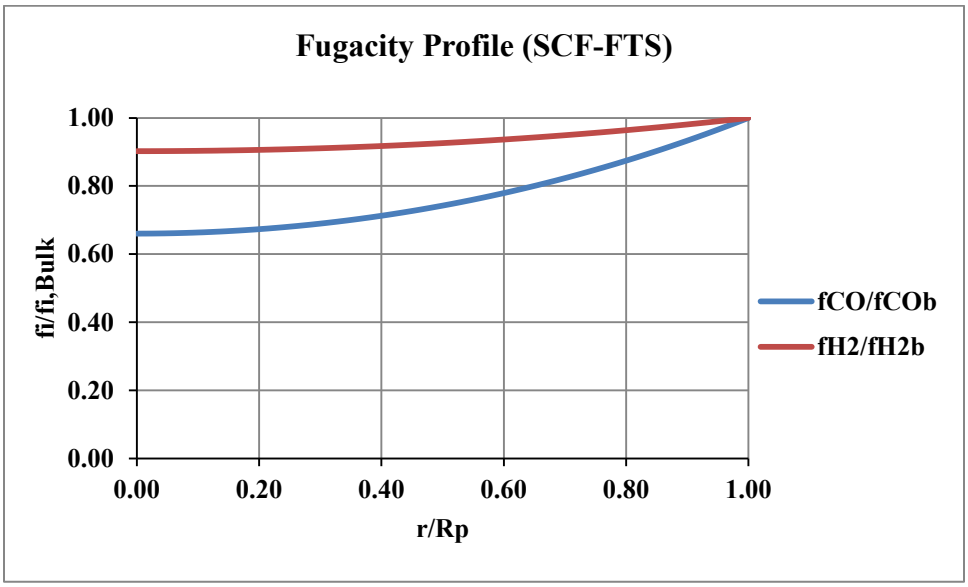

Figure 5.1: Dimensionless concentration profiles inside catalyst pellet under SCF-FTS (temperature: 513 K; pressure: 80 bar; syngas ratio (H_2/CO): 2:1; solvent/syngas ratio: 3; pellet diameter: 1mm)

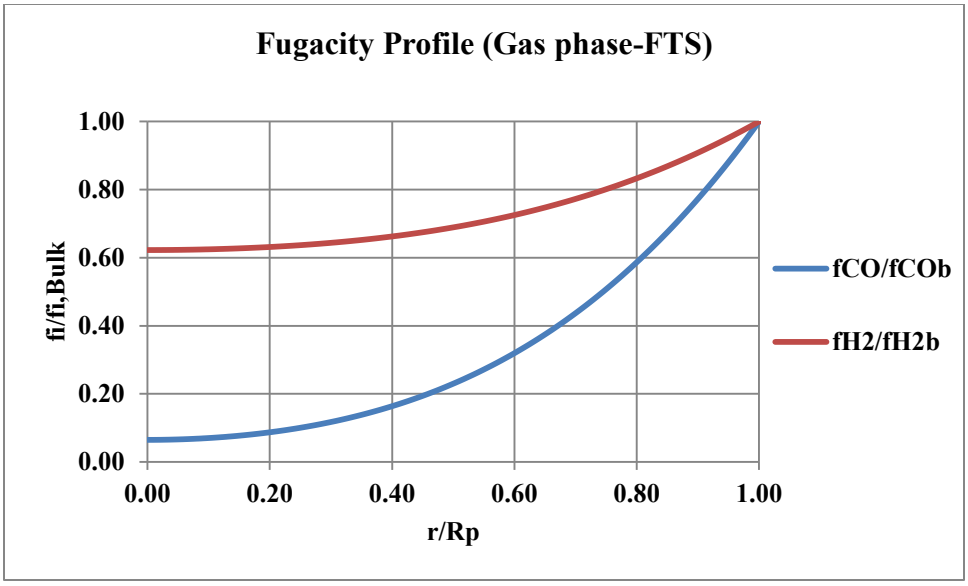

Figure 5.2: Dimensionless concentration profiles within catalyst pores under gas-phase FTS (temperature: 513 K; pressure: 80 bar; syngas ratio (H_2/CO): 2:1; Nitrogen/syngas ratio: 3; pellet diameter: 1mm)

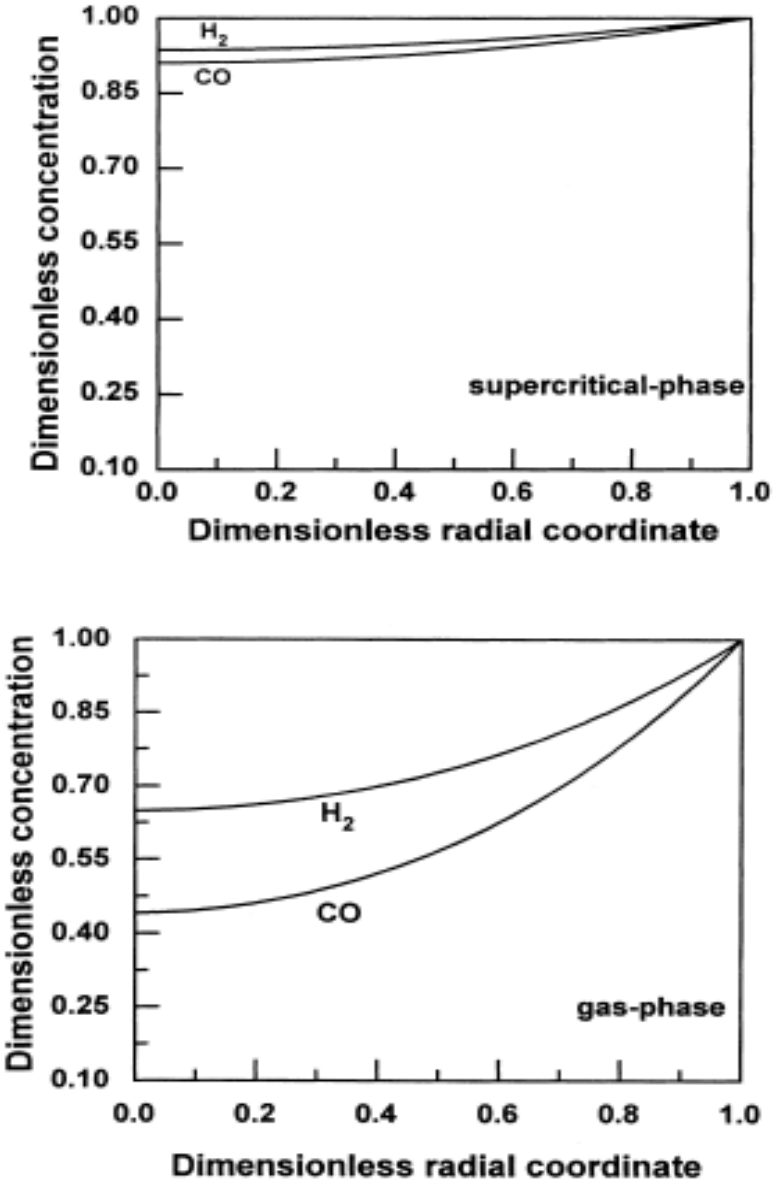

Figure 5.3: Reactants concentration profiles within catalyst pores in SCF and in gas-phase using Co/SiO_2 catalyst (particle size=0.9 mm, T=210°C, P=35 bar) [50]

5.1.3 Pressure-Tuning Effect on SCF-FTS

The following are the concentration profiles inside the catalyst pore under SCF-FTS at different operating pressures (35, 65 and 80 bar) to investigate the effect of pressure tuning in the critical and near the critical phase and also to study the effect of diffusion on the performance of the catalyst pellet.

In Figure 5.4 and Figure 5.5, as the total pressure increases from 35 bar to 80 bar, the system moves from the gas-phase to the liquid-phase and then to the SCF by simply tuning the operating pressure. These figures also show the influence of pressure on reactant conversion in the SCF-FTS. It was observed that the reactant conversion decreases with increasing the pressure, since the bulk diffusivity decreases when increasing the pressure. This means that at high pressure, external diffusion limitations control the process.

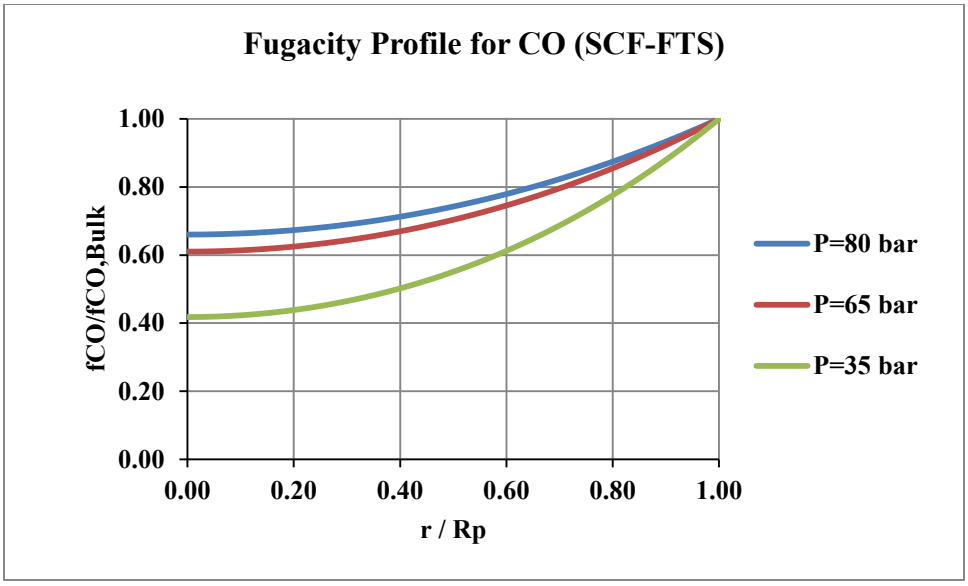

Figure 5.4: Carbon monoxide concentration profile inside the catalyst pores under the SCF-FTS conditions under different total pressures (temperature =250^{o}C, solvent/syngas ratio = 3 and H_2/CO ratio = 2)

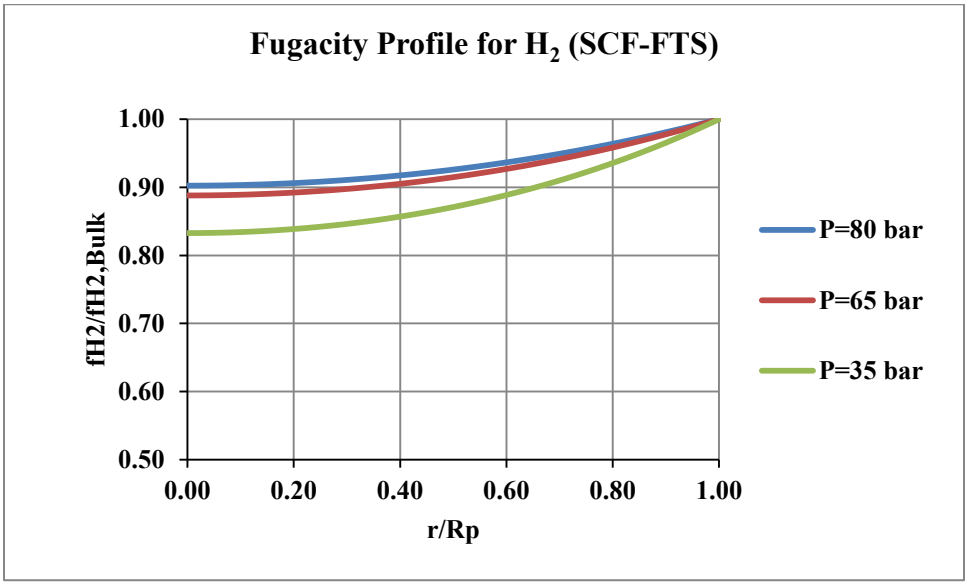

Figure 5.5: Hydrogen concentration profile inside the catalyst pores under the SCF-FTS conditions under different total pressures (temperature =250^{o}C, solvent/syngas ratio = 3 and H_2/CO ratio = 2)

5.1.4 Particle Size Effect on SCF-FTS

A simulation of the effect of the catalyst particle size on the overall catalyst effectiveness factor for both reaction media is shown in the following Figure 5.6. In the SCF-FTS, as the diameter of the catalyst pellet increased from 1 mm to 5 mm, the overall catalyst effectiveness factor decreased from 0.99 to 0.86. While in the gas-phase FTS, the overall effectiveness factor sharply dropped from 0. 96 to 0.75.

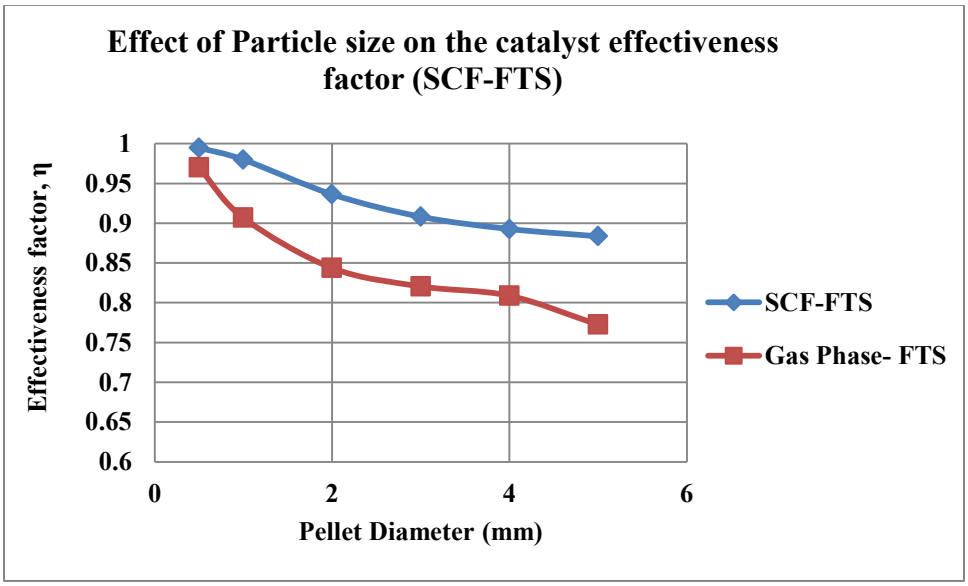

Figure 5.6: Modeling of the effect of the catalyst pellet size on the overall effectiveness factor

5.1.5 Temperature Profile

The following Figure 5.7 shows the temperature profile inside the catalyst pellet. As can be noticed, there no was significant increase in the temperature inside the catalyst pellet (i.e., the temperature difference was found to be less than 1°C.). This indicates that the heat generated during the exothermic reaction is transferred by conduction from the catalyst pore to the outer surface of the catalyst and by convection from the outer catalyst surface to the bulk fluid (i.e., isothermal catalyst pellet).

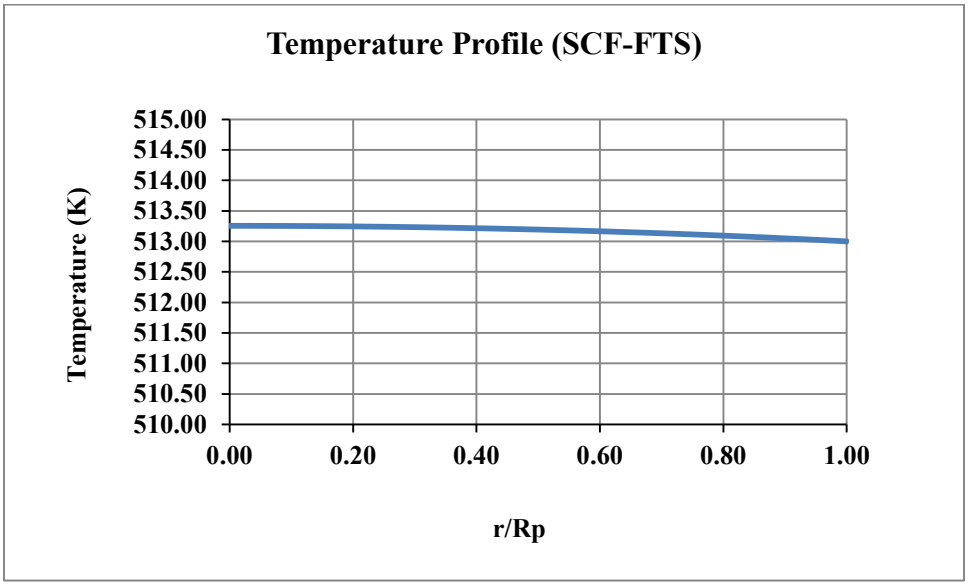

Figure 5.7: Temperature profiles within catalyst pores under SCF-FTS (temperature: 513 K; pressure: 80 bar; syngas ratio (H_2/CO): 2:1; solvent/syngas ratio: 3; pellet diameter: 1mm)

5.2 Macro-scale Modeling

5.2.1 Conversion Profile

Figure 5.4 and Table 5.1 present the effects of reaction media on the CO conversion level. Since the reactant mass diffusivity rates are higher in the gas-phase than in the SCF-FTS, it might be expected that a higher CO conversion would be obtained under the conventional gas-phase reaction. However, the modeling results presented in Figure 5.8 show significantly higher CO conversions under SCF–FTS (ca.78 %) relative to the gas-phase FTS (ca.69 %) at the same total pressure (80 bar).

In the gas-phase FTS reaction, under the steady state operation, the catalyst pores are filled with the heavy liquid hydrocarbons in which the reactants must be dissolved and then diffuse to reach the catalyst active sites. While in the SCF-FTS, it is well known that SCF have high solubility which can enhance the *in-situ* extraction of heavy hydrocarbons.

Accordingly, the transportation of the reactants to the catalyst surface is facilitated and the CO conversion is consequently increased [23, 50, 51].

Huang and Roberts [23], Irankhah and Haghtalab [52] and Yan et al. [50] reported similar experimental observations using a cobalt based catalyst with different total pressure, as shown in Table 5.2.

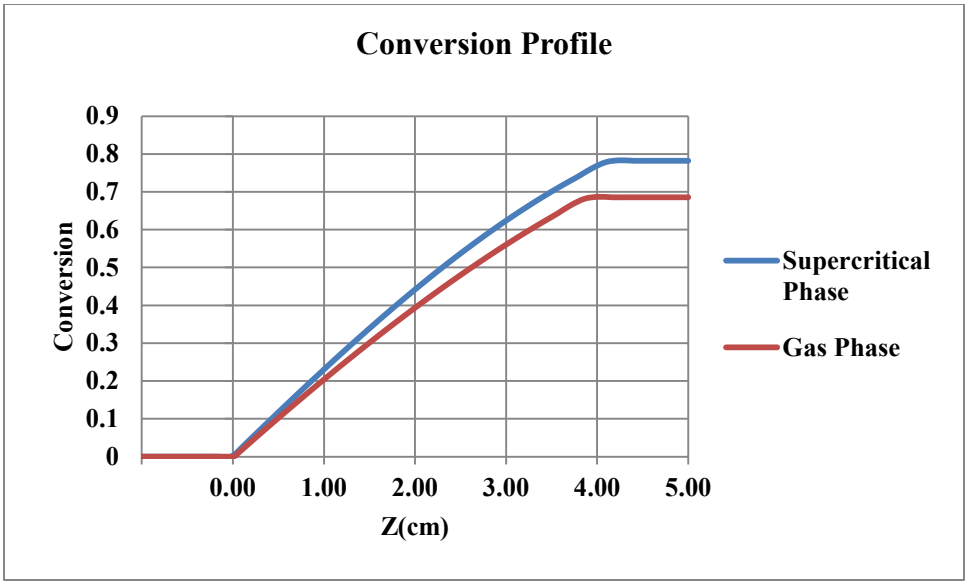

Figure 5.8: Conversion profile under SCF phase and gas phase (feed temperature: 513 K; pressure: 80 bar; syngas ratio (H_2/CO): 2:1; Nitrogen to syngas ratio: 3:1)

Table 5.2: Comparison of the CO conversion level for both SCF- and gas-phase FTS

Phase	T (◦C)	P (bar)	CO/H2	X_{CO} (%)	Catalyst	Ref.
Gas	210	45	1/2	70	Co/SiO2	[50]
SCF	210	45	1/2	84		
Gas	250	20	1/2	50	Co-Pt/Al2O3	[23]
SCF	250	80	1/2	70		
Gas	240	55	1/2	54	Co-Ru/Al2O3	[52]
SCF	240	55	1/2	63		
Gas	240	80	1/2	69	Co/Al2O3	This work
SCF	240	80	1/2	78		

5.2.2 Temperature Profile

The temperature distribution was investigated along the length of the reactor for both SCF-FTS and gas-phase FTS (Figure 5.9). Under a supercritical-phase reaction, the temperature profile is significantly flatter along the reactor compared to the gas-phase reaction. This shows that the supercritical media is more efficient in absorbing and distributing the heat generated by the exothermic reaction. The maximum temperature rise along the catalyst bed in the SCF-FTS is around 5 °C, while it is around 10 °C in the gas-phase FTS. These results suggest that the heat transfer rate is more effective in the SCF-FTS compared to the gas-phase FTS reaction. This is due to the high heat capacity of the solvent that influences the heat transfer rate. In addition, the thermal conductivity of many gases, including light hydrocarbons, increases significantly by 5 or 6 times in the SCF-FTS compared to the conventional gas-phase FTS [53].

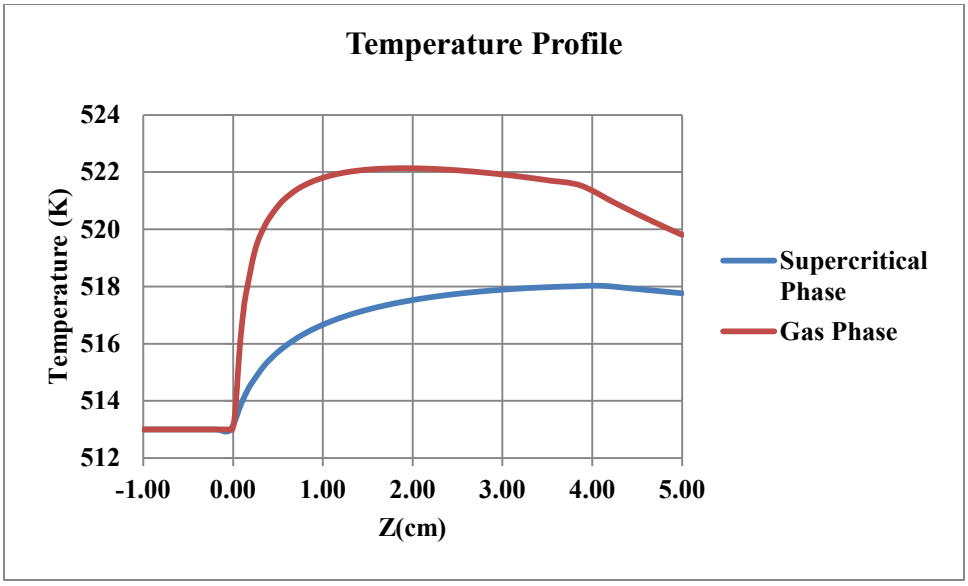

Figure 5.9: Temperature distribution under SCF phase and gas phase (feed temperature: 513 K; pressure: 80 bar; syngas ratio (H_2/CO): 2:1; solvent to syngas ratio: 3:1)

The temperature distribution was done experimentally by Yokota and Fujimoto [37] using supported silica cobalt catalyst (Co-La/SiO_2). They reported that the temperature rise is 10 ˚C, 13 ˚C and 18 ˚C in the liquid-, SCF- and gas-phase FTS reaction, respectively (see Figure 5.10a), using different total pressure (45 bar) and solvent/syngas ratios (*n*-Hexane/syngas=3). Also, another study by Irankhah and Haghtalab [52] shows that the maximum temperature rises using cobalt based catalyst (Co-Ru/Al_2O_3) were 7 ◦C and 15 ◦C in the SCF-FTS and gas-phases FTS, respectively, using different total pressure (55 bar) (Figure 5.10c). Similar results were shown by Huang and Roberts [23] using a cobalt-based catalyst (15% Co-0.5% Pt/Al_2O_3) under reaction conditions similar to this study. They stated that the maximum temperature deviation is 5 ˚C in the SCF-FTS compared to 15 ˚C in the gas-phase FTS (Figure 5.10b).

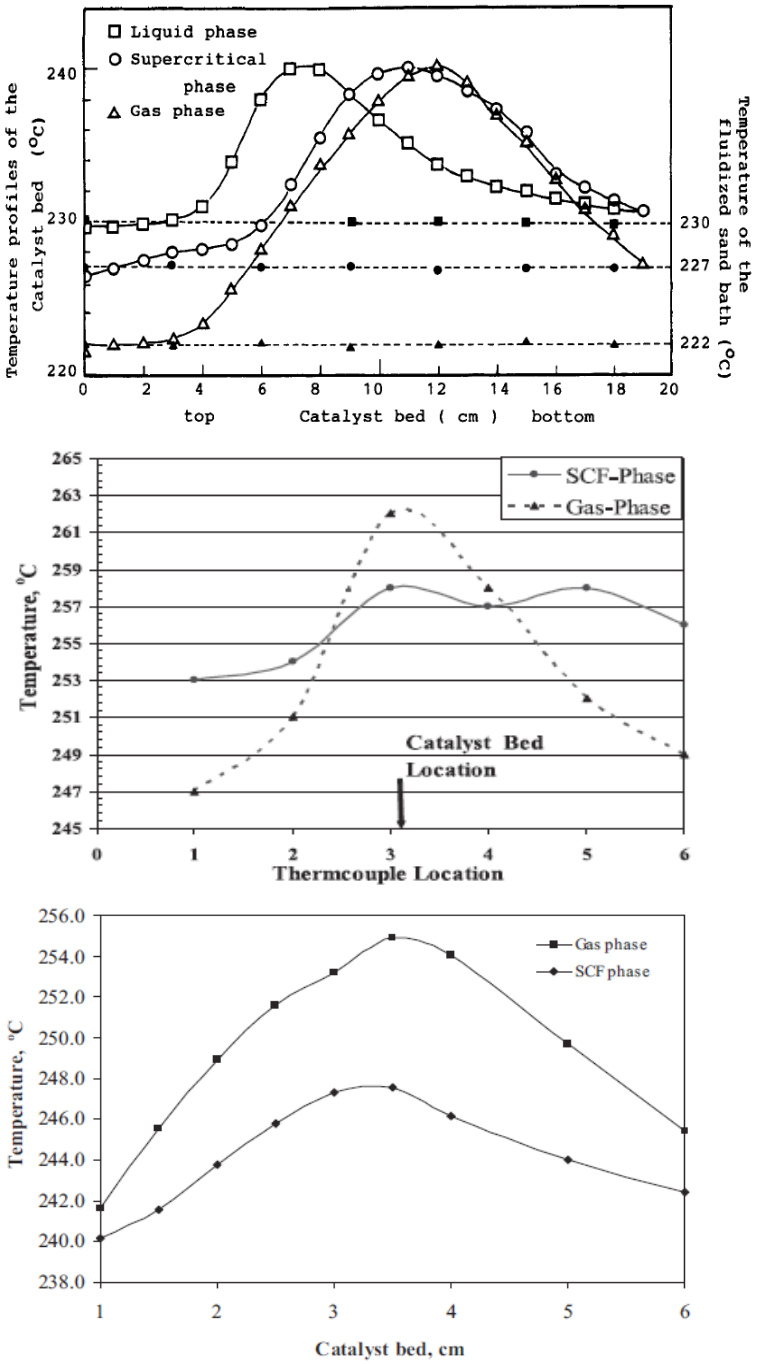

Figure 5.10: Experimental temperature profile under SCF- and gas- phase FTS (a) Yokota and Fujimoto) [37], (b) Huang and Roberts [23] and (c) Irankhah and Haghtalab [52]

5.2.3 Comparison of the Catalyst Effectiveness Factor

The following Figure 5.11 shows the relation between the overall catalyst effectiveness factor and CO conversion for the conventional gas-phase and SCF-FTS. The results show high effectiveness factor in both reaction media until a certain conversion (around 50%). However, the overall catalyst effectiveness factor of the gas-phase FTS drops dramatically from 0.9 to 0.75 above a certain conversion (from 50% to 80 %). The overall effectiveness factor at the SCF-FTS shows almost a constant pattern at all conversion levels (η is almost equal to 1) which indicates that there is no mass transfer resistance and that the overall effectiveness factor is equal to the internal effectiveness factor. Similar findings were reported by Elbashir et al. [8], assuming that the pores in the gas-phase FTS are filled with the gaseous reactants, while in this work the pores are assumed to be filled with the heavy wax represented by *n*-$C_{28}H_{58}$.

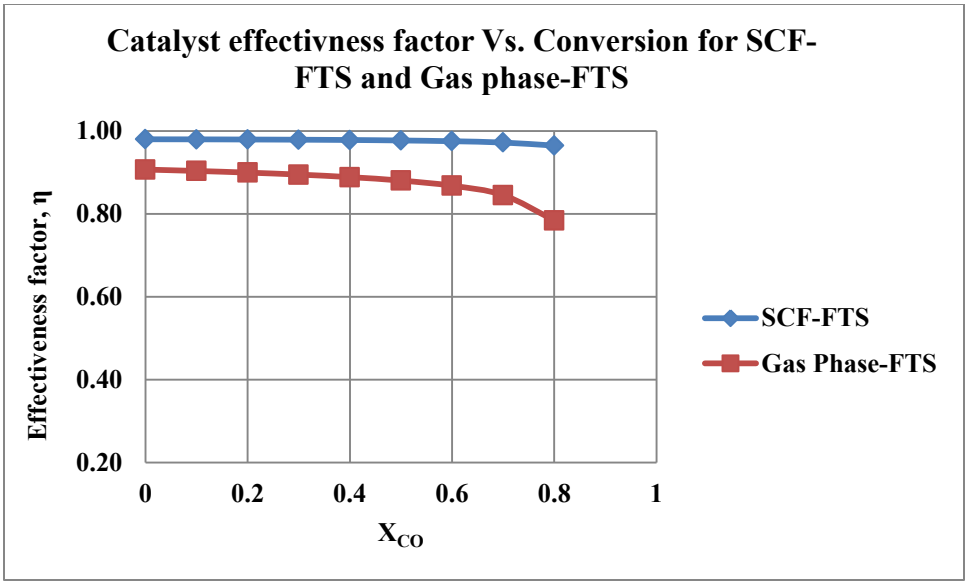

Figure 5.11: The catalyst effectiveness factor at different CO conversions for the conventional gas phase and SCF- FTS filled (temperature =250 ^{o}C bar, solvent/syngas ratio = 3 and H_2/CO ratio = 2)

6. CONCLUSION AND RECOMMENDATIONS

In conclusion, this study provided a framework to understand the performance of SCF-FTS. A one-dimensional heterogeneous model has been developed to simulate temperature and concentration profiles simultaneously in a fixed-bed reactor under both gas-phase and SCF-FTS. In the modeling process a comprehensive catalyst pellet was used to simulate the diffusion and reaction in a typical spherical catalyst pellet. A fugacity-based kinetic model was implemented into the reactor model along with considering the assumption that the catalyst pores would be filled with liquid wax (for the case of conventional gas-phase-FTS) and with supercritical *n*-Hexane (for the case of SCF-FTS) under realistic operating conditions for the reaction. The thermodynamic properties of the reaction mixture were calculated by using SRK-EOS. The reactor model was validated using the data reported from the experimental investigation available in the literature, and satisfactory agreements were found between the model prediction and experimental results for similar conditions. MATLAB was used to solve the system of ODEs using ode45 function.

The simulation results provide a prediction for the effect of major variables such as temperature, pressure and pellet size on the reaction behavior. It was observed that the syngas conversion can be enhanced in the SCF-FTS compared to the gas-phase FTS. Additionally, the simulation in both reaction media indicated that, the increase of reaction operating pressure has a significant effect on the increase of CO conversion at certain conditions. semi flat temperature profile was obtained under CF-FT

reaction with a temperature rise of 5 C. However, in the gas-phase reaction the temperature profile showed a very sharp increase in temperature (around 1 C) in the first two centimeters of the reactor bed. This result is in agreement with the previous experimental reporting in this regard [37, 46, 50, 52].

The overall catalyst effectiveness factor was higher in the gas-phase FTS compared to the SCF-FTS at the entrance of the reactor bed however the effectiveness factor for the SCF become superior at the middle and the bottom of the reactor bed. The decrease of the catalyst effectiveness factor for the gas-phase FTS can be implemented to formation of the wax as result product condensation inside the pores, which result in enhancing the mass transfer limitation. However, in the SCF-FTS the catalyst effectiveness factor shows a small variation as the conversion increased along the bed length because of the *in-suit* extraction of the heavy hydrocarbons by the solvent. Moreover, our findings show that the pellet size had an important effect on the overall catalyst effectiveness factor. The catalyst effectiveness factor showed a clearly decreasing trend as the diameter of the particle increased.

Future work can be done to improve the research work conducted and presented in this thesis. This model can be extended to other kinetic models, equations of state, catalyst types or operating conditions. The modeling studies could as well include the overall product distribution of the hydrocarbons obtained from the FTS on both gas-phase and the SCF media. Future research could also focus on developing a better represented EOS for the non-ideal behavior of the reaction mixture under the high pressure FTS conditions. Experimental data could be used to validate and further

improve the model using our new bench-scale fixed-bed reactor installed recently at Texas A&M University at Qatar. More importantly, the visualization of the reactor *in-situ* behavior will be conducted utilizing advanced MRI and NMR faculties at the University of Cambridge could as well provide accurate measurements of diffusivities and other transport properties.

REFERENCES

[1] R. Chedid, M. Kobrosly and R. Ghajar, Energy Policy, 35 (2007) 4799.

[2] L. Fan and K. Fujimoto, Applied Catalysis A: General, 186 (1999) 343.

[3] L. Fan, K. Yokota and K. Fujimoto, Aiche J, 38 (1992) 1639.

[4] L. Fan, K. Yokota and K. Fujimoto, Top Catal, 2 (1995) 267.

[5] H. Kolbel and M. Ralek, Catal Rev, 21 (1980) 225.

[6] R.M. Malek Abbaslou, J.S. Soltan Mohammadzadeh and A.K. Dalai, Fuel Process Technol, 90 (2009) 849.

[7] D. Stern, A.T. Bell and H. Heinemann, Chem Eng Sci, 38 (1983) 597.

[8] A.K. Mogalicherla, E.E. Elmalik and N.O. Elbashir, Chemical Engineering and Processing: Process Intensification, 62 (2012) 59.

[9] S.T. Sie and R. Krishna, Appl Catal a-Gen, 186 (1999) 55.

[10] N.O. Elbashir, D.B. Bukur, E. Durham and C.B. Roberts, Aiche J, 56 (2010) 997.

[11] X. Lang, A. Akgerman and D.B. Bukur, Ind Eng Chem Res, 34 (1995) 72.

[12] K. Yokota, Y. Hanakata and K. Fujimoto, Fuel, 70 (1991) 989.

[13] E.F. Sousa-Aguiar, L.G. Appel and C. Mota, Catalysis Today, 101 (2005) 3.

[14] P.L. Spath, Dayton, D.C., Preliminary Screening —Technical and Economic Assessment of Synthesis Gas to Fuels and Chemicals with Emphasis on the Potential for Biomass-Derived Syngas, Golden, Colo. : National Renewable Energy Laboratory 2003.

[15] N.O. Elbashir and C.B. Roberts, Ind Eng Chem Res, 44 (2005) 505.

[16] G. Bub, M. Baerns, B. Bussemeier and C. Frohning, Chem Eng Sci, 35 (1980) 348.

[17] E.S. Lox and G.F. Froment, Ind Eng Chem Res, 32 (1993) 61.

[18] B. Sarup and B.W. Wojciechowski, Can J Chem Eng, 67 (1989) 62.

[19] G.P. Van der Laan and A.A.C.M. Beenackers, Catal Rev, 41 (1999) 255.

[20] I.C. Yates and C.N. Satterfield, Energ Fuel, 5 (1991) 168.

[21] B.W. Wojciechowski, Catal Rev, 30 (1988) 629.

[22] A.O.I. Rautavuoma and H.S. Vanderbaan, Appl Catal, 1 (1981) 247.

[23] X.W. Huang and C.B. Roberts, Fuel Process Technol, 83 (2003) 81.

[24] A.K. Mogalicherla and N.O. Elbashir, Energ Fuel, 25 (2011) 878.

[25] B.H. Davis, Catalysis Today, 71 (2002) 249.

[26] A. Mena Subiranas, Combining Fischer-Tropsch Synthesis (FTS) And Hydrocarbon eactions n One eactor, niv ersit tsve rlag arlsruhe, a rlsruhe, 2008.

[27] D.B. Bukur, X.S. Lang, A. Akgerman and Z.T. Feng, Ind Eng Chem Res, 36 (1997) 2580.

[28] N.O. Elbashir, P. Dutta, A. Manivannan, M.S. Seehra and C.B. Roberts, Appl Catal a-Gen, 285 (2005) 169.

[29] Y.N. Wang, Y.Y. Xu, Y.W. Li, Y.L. Zhao and B.J. Zhang, Chem Eng Sci, 58 (2003) 867.

[30] A. Jess and C. Kern, Chem Eng Technol, 32 (2009) 1164.

[31] L. Quan-Sheng, Z. Zhi-Xin and Z. Jing-Lai, Natural Gas Chemistry, 8 (1999) 137.

[32] A. Moutsoglou and P.P. Sunkara, Energ Fuel, 25 (2011) 2242.

[33] K.M. Brunner, J.C. Duncan, L.D. Harrison, K.E. Pratt, R.P.S. Peguin, C.H. Bartholomew and W.C. Hecker, Int J Chem React Eng, 10 (2012).

[34] A. Baiker, Chem Rev, 99 (1999) 453.

[35] G. Brunner, Gas extraction: an introduction to fundamentals of supercritical fluids and the application to separation processes, Darmstadt: Steinkopff Verlag ; New York: Steinkopff Verlag 2004.

[36] M. McCoy, Chem Eng News, 77 (1999) 11.

[37] K. Yokota and K. Fujimoto, Ind Eng Chem Res, 30 (1991) 95.

[38] K. Yokota, Y. Hanakata and K. Fujimoto, Chem Eng Sci, 45 (1990) 2743.

[39] H. Scott Fogler, Elements of chemical reaction engineering, Upper Saddle River, NJ : Prentice Hall PTR 2006.

[40] C.H. He, Aiche J, 43 (1997) 2944.

[41] Y.N. Wang, Y.Y. Xu, H.W. Xiang, Y.W. Li and B.J. Zhang, Ind Eng Chem Res, 40 (2001) 4324.

[42] G.H. Charles, An Introduction to Chemical Engineering Kinetics and Reactor Design, John Wiley & Sons, Inc, 1977.

[43] J. Wu, H. Zhang, W. Ying and D. Fang, Int J Thermophys, 31 (2010) 556.

[44] Y. Arai, Sako, T. , Takebayashi,Y. , Supercritical Fluids: Molecular Interactions, Physical Properties, and New Applications (Springer Series in Material

Processing). Edited by Yasuhiko Arai, Takeshi Sako, and Yoshihiro Takebayashí, Springer, 2001.

[45] T.p.o.g.a. liquids, The properties of gases and liquids, New York : McGraw-Hill 1987.

[46] M.E. Davis, R. J. Davis Fundamentals of chemical reaction engineering, McGraw-Hill Boston, 2003.

[47] G.F. Froment, Bischoff, K.B ., Chemical reactor analysis and design, Wiley 2011.

[48] A.P. de Wasch and G.F. Froment, Chem Eng Sci, 27 (1972) 567.

[49] R.J. Madon and E. Iglesia, Journal of Catalysis, 149 (1994) 428.

[50] S.R. Yan, L. Fan, Z.X. Zhang, J.L. Zhou and K. Fujimoto, Appl Catal a-Gen, 171 (1998) 247.

[51] B. Subramaniam, Appl Catal a-Gen, 212 (2001) 199.

[52] A. Irankhah and A. Haghtalab, Chem Eng Technol, 31 (2008) 525.

[53] N.V. ëTìSederberg, Thermal conductivity of gases and liquids, M.I.T. Press, Cambridge, 1965.

APPENDIX A

DERIVATION OF THE DIFFERENTIAL EQUATION FOR MASS AND HEAT

To derive the concentration profile of reactants by performing a steady-state mole balance on a species i in a spherical catalyst shell of an inner radius r and outer radius $r + \Delta r$ (Figure A.1)

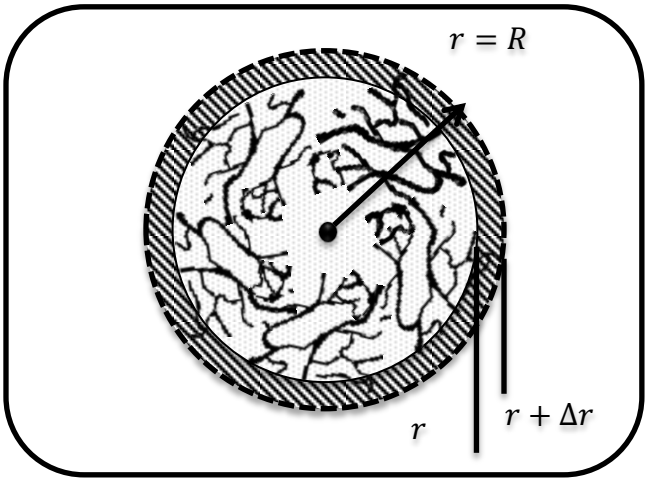

Figure A.1: Catalyst pellet shell balance

$Rate\ of\ reactant\ i\ in\ at\ r = W_i.Area = W_i \times 4\pi r^2|_r$

$Rate\ of\ reactant\ i\ out\ at\ (r + \Delta r) = W_i.Area = W_i \times 4\pi r^2|_{r+\Delta r}$

$Rate\ of\ generation\ of\ i\ within\ the\ shell\ thickness\ \Delta r = r_i \times \rho_{cat.} \times 4\pi r^2 \Delta r$

where W_i is the flux, r_i is the rate of reaction per unit mass of catalyst and $\rho_{cat.}$ is the density of the pellet.

Then, the molar balance over the shell thickness is:

$$In - Out + Generation = 0$$

$$(W_i \times 4\pi r^2|_r) - (W_i \times 4\pi r^2|_{r+\Delta r}) + (r_i \times \rho_{cat.} \times 4\pi r^2 \Delta r) = 0$$

Dividing by $(-4\pi\Delta r)$ and taking the limit as $\Delta r \to 0$, the following differential equation is obtained:

$$\frac{d(W_i r^2)}{dr} + (-r_i)\rho_{cat.} r^2 = 0 \qquad \text{Equation A.1}$$

For equal molar counter diffusion, the molar flus is:

$$W_i = -D_i^e \frac{dC_i}{dr} \qquad \text{Equation A.2}$$

where C_i is the concentration of component i.

After substituting equation A.2 into equation A.1, the following differential equation is obtained to describe the diffusion and reaction inside the catalyst pellet

$$\frac{d\left[-D_i^e \left(\frac{dC_i}{dr}\right) r^2\right]}{dr} + (-r_i)\rho_{cat.} r^2 = 0 \qquad \text{Equation A.3}$$

Rearranging equation A.3

$$\frac{D_i^e}{r^2} \frac{d}{dr}\left(r^2 \frac{dC_i}{dr}\right) = (-r_i)\rho_{cat} \qquad \text{Equation A.4}$$

The fugacity based mass balance was estimated for the previous equation A.4 to account for the no ideality for the system by utilizing the real gas low equation as follows:

$$PV = znRT \qquad \text{Equation A.5}$$

where P is the pressure, V is the volume, z is the compressibility factor and n is the number of moles.

From the definition of partial pressure, the partial pressure of component i in the gas mixture is the total pressure times the mole fraction of that component:

$$P_i = y_i P \qquad \text{Equation A.6}$$

Then,

$$P_i V = z n_i RT \qquad \text{Equation A.7}$$

Then, $P_i = zC_i RT$, $where\ C_i = {}^{n_i}/_{V}$

where P_i is the partial pressure for component i and n_i is the number of moles component i.

The fugacity coefficient for a component in a mixture is defined as follows:

$$\Phi_i = \frac{f_i}{y_i P} \qquad \text{Equation A.8}$$

where f_i and Φ_i are the fugacity and fugacity coefficient of component i in the mixture.

After substituting equation A.8 into equation A.7, and solving for concentration, the following expression is obtained:

$$C_i = \frac{p_i}{zRT} = \frac{f_i}{\Phi_i zRT}$$

Then the differential equation (equation A.4), is written in terms of fugacity assuming that Φ_i is constant in the radial direction is as the following:

$$\frac{D_i^e}{r^2}\frac{d}{dr}\left(r^2\frac{df_i}{dr}\right) = \Phi_i zRT(-r_i)\rho_{cat} \qquad \text{Equation A.9}$$

Applying the chain rule on the previous equation A.9 gives:

$$\frac{d^2 f_i}{dr^2} + \frac{2}{r}\frac{df_i}{dr} = \frac{\Phi_i z R T (-r_i)\rho_{cat}}{D_i^e}$$ Equation A.10

APPENDIX B

THE CALCULATION OF MASS AND HEAT TRANSFER COEFFICIENT

B.1. External Mass Transfer Coefficient

The external mass transfer coefficient is related to binary diffusion confident, particle diameter and Sherwood number as per the following equation [39]:

$$sh = \frac{k_c\, d_p}{D_{AB}} \qquad \text{Equation B.1}$$

where, sh is Sherwood number, k_c is the mass transfer coefficient (cm/s), d_p is the diameter of the pellet (cm) and D_{AB} is the mass diffusivity of CO in the supercritical hexane (cm^2/s).

Then, the correlation for mass transfer flow around spherical catalyst pellets is given by Frossling correlation that was developed by Frossling et al. [39]:

$$sh = 2 + 0.6\, Re^{1/2}\, Sc^{1/3} \qquad \text{Equation B.2}$$

where R_e is Reynolds number and S_C is Schmidt number.

$$Sc = \frac{\nu}{D_{AB}} \qquad \text{Equation B.3}$$

$$Re = \frac{\rho\, d_p u}{\mu} \qquad \text{Equation B.4}$$

where, ν is momentum diffusivity (cm^2/s), ρ is the fluid density (g/cm^3), u is the free-stream velocity (cm/s) and μ is the viscosity for supercritical hexane (C_p).

B.2. Data Used and Sample Calculation

The physical properties (i.e. viscosity, density and kinematic viscosity) were estimated using Aspen Plus® simulation package at $T = 513\ K$ and $P = 80\ bar$ for the

bulk fluid (*n*-Hexane) using SRK-EOS (see Table B.1). The calculation for binary diffusion coefficient of CO in the bulk fluid (*n*-Hexane), $D_{CO-Hexane}$, is given in Appendix C.

Table B.1: Solvent physical properties used for the calculation

Viscosity, μ	5.36E-04 g/cm.s
Density, ρ	0.3730 g/cm^3
kinematic viscosity, ν	1.44E-03 cm^2/s
$D_{CO-Hexane}$	1.03E-03 cm^2/s
Pellet diameter, d_p	0.1 cm
Velocity, U	0.15 cm/s

$$Re = \frac{\rho\, d_p U}{\mu} = \frac{(0.3730\,)(0.1)(0.15)}{(5.36 \times 10^{-4})} = 10.54$$

$$Sc = \frac{\nu}{D_{AB}} = \frac{(1.44 \times 10^{-3})}{(1.03 \times 10^{-3})} = 1.93$$

$$sh = 2 + 0.6\, Re^{1/2}\, Sc^{1/3} = 2 + 0.6(10.54)^{1/2}(1.93)^{1/3} = 4.17$$

$$k_c = \frac{sh\, D_{AB}}{d_p} = \frac{(1.93)(1.03 \times 10^{-3})}{(0.1)} = 4.30 \times 10^{-2}\ cm^2/s = 4.30 \times 10^{-4}\ m^2/s$$

B.3. Heat Transfer Coefficient

The heat transfer coefficient is related to thermal conductivity, particle diameter and Nusselt number as follows [39]:

$$Nu = \frac{h\, d_p}{\lambda_{fluid}}$$ Equation B.5

where, Nu is Nusselt number, h is the heat transfer coefficient (W/ cm^2.K), d_p is the diameter of the pellet (cm) and λ_{fluid} is the thermal conductivity of the bulk fluid (W/cm.s).

Then, the correlation that relates the Nusselt number to Prandtl number for a flow around a spherical catalyst pellet is given by Ranz et al. [39]:

$$Nu = 2 + 0.6\, Re^{1/2}\, Pr^{1/3}$$ Equation B.6

$$Pr = \frac{\mu C_p}{\lambda_{fluid}}$$ Equation B.7

where Pr is the Prandtl number and C_p is the heat capacity (J/g.K).

B.4. Data Used and Sample Calculation

The heat capacity was estimated using Aspen Plus® simulation package at $T = 513\, K$ and $P = 80\, bar$ for the bulk fluid (n-Hexane) using SRK-EOS. The calculation for thermal conductivity of the bulk fluid (n-Hexane) is given in Appendix D.

Table B.1: Fluid Heat capacity and thermal conductivity

Heat capacity, C_p	3.7343 J/g.K
Thermal conductivity, λ_{fluid}	5.84E-02 W/m.K

$$Re = \frac{\rho\, d_p U}{\mu} = \frac{(0.3730\ )(0.1)(0.15)}{(5.36 \times 10^{-4})} = 10.54$$

$$Pr = \frac{\mu C_p}{\lambda_{fluid}} = \frac{(5.36 \times 10^{-4})(3.7343)}{(5.84 \times 10^{-2})} = 3.42$$

$$Nu = 2 + 0.6\, Re^{1/2}\, Pr^{1/3} = 2 + 0.6(10.54)^{1/2}(3.42)^{1/3} = 4.92$$

$$h = \frac{Nu\ \lambda_{fluid}}{d_p} = \frac{(4.92)(5.84 \times 10^{-2})}{(0.1)} = 287.5\ W/m^2.K$$

APPENDIX C

THE CALCULATION OF BINARY DIFFUSION COEFFICIENT AND EFFECTIVE MASS DIFFUSIVITY

C.1. Data Used and Sample Calculation

Properties estimated from Aspen Plus utilizing the SRK-EOS for *n*-Hexane (1) and CO (2) as the following:

Table C.1: Operating conditions and catalyst physical properties

Temperatures, T	513 K
Total Pressure, P	80 bar
H_2/CO feed ratio, V	2
Hexane/Syngas ratio, S	3
Pellet diameter, d_{Pellet}	1 mm
Pellet radius, R_{Pellet}	0.05 cm
Pellet porosity, ε_p	0.5
Pellet density, ρ_{cat}	1.5 g/cm^3
Pellet tortuosity,τ	3
Mean pore diameter, d_P	114.8 Å
Molecular weight, M_{W1}	86 g/mol
Molecular weight, M_{W2}	28 g/mol
Critical pressure, P_{C1}	30.25 bar
Critical volume, V_{C1}	371 cm^3/mol
Critical volume, V_{C2}	94.4 cm^3/mol
Critical density, ρ_{C1}	0.0027 mol/cm^3

Density, ρ_1 at 80 bar and 513 K	0.0048 mol/cm^3
Molar volume at 80 bar and 513 K, V_1	209.34 cm^3/mol

The Molecular diffusivity of hydrogen and CO has been determined by using the following equation:

$$D_{21} = \left[0.61614 + 3.0902 * \exp\left(-0.87756\frac{\sqrt{M_1 V_{C1}}}{P_{C1}}\right)\right] * 10^{-6}\left(V_1^k - 23\right) * \sqrt{\frac{T}{M_2}}$$

$$\rho_r = {}^{\rho_1}/_{\rho_{C1}} = {}^{V_{C1}}/_{V_1}$$

$$\rho_r = {}^{V_{C1}}/_{V_1} = {}^{371}/_{209.34} = 1.77 > 1.2 \rightarrow k = 1$$

Molecular diffusivity of CO in *n*-hexane

$$D_{CO-Hexane} = \left[0.61614 + 3.0902 * \exp\left(-0.87756\frac{\sqrt{86 * 371}}{30.25}\right)\right]$$

$$* 10^{-6}(209.34 - 23) * \sqrt{\frac{513}{28}} = 1.03 \times 10^{-3}\ cm^2/s$$

Molecular diffusivity of hydrogen in *n*-hexane

$$D_{H_2-Hexane} = \left[0.61614 + 3.0902 * \exp\left(-0.87756\frac{\sqrt{86 * 371}}{30.25}\right)\right]$$

$$* 10^{-6}(209.34 - 23) * \sqrt{\frac{513}{2}} = 3.86 \times 10^{-3}\ cm^2/s$$

Effective diffusivity of CO and H_2 are calculated as the following:

$$D^{e}_{CO-Hexane} = \frac{D_{CO-Hexane}\ \varepsilon_P}{\tau} = \frac{(1.03 \times 10^{-3})\ (0.5)}{(3)} = 1.33 \times 10^{-4}\ cm^2/s$$

$$D^{e}_{H_2-Hexane} = \frac{D_{H_2-Hexane}\varepsilon_P}{\tau} = \frac{(3.86 \times 10^{-3})(0.5)}{(3)} = 6.43 \times 10^{-4}\ cm^2/s$$

APPENDIX D

THE CALCULATION OF THERMAL CONDUCTIVITY

D.1. Thermal Conductivity of *n*-Hexane using Stiel and Thodos Correlations

The thermal conductivity of the bulk fluid, which is *n*-Hexane in our case, could be calculated by the correlation developed by Stiel and Thodos as follows [45]:

$$(\lambda_m - \lambda_m^o)\Gamma z_c^5 = 14.0 \times 10^{-8}[\exp(0.535\,\rho_r) - 1] \quad for \quad \rho_r < 0.5 \qquad \text{Equation D.1}$$

$$(\lambda_m - \lambda_m^o)\Gamma z_c^5 = 13.1 \times 10^{-8}[\exp(0.67\,\rho_r) - 1.069] \quad for\ 0.5 < \rho_r < 2.0 \qquad \text{Equation D.2}$$

$$(\lambda_m - \lambda_m^o)\Gamma z_c^5 = 2.976 \times 10^{-8}[\exp(1.155\,\rho_r) + 2.016] \quad for\ 2.0 < \rho_r < 2.8 \qquad \text{Equation D.3}$$

where λ_m and λ_m^o are in cal/cm s K, Γ is the reduced inverse thermal conductivity $(W/m.K)^{-1}$

D.2. Thermal Conductivity of *n*-Hexane using Aspen

The steps used to calculate the thermal conductivity as a function of temperature using linear regression:

1. Use Aspen physical properties system was used to calculate *n*-Hexane thermal conductivity utilizing SRK-EOS at different temperature and pressure.
2. Fit the following polynomial equation, by assuming a random values for a,b and c.

$$\lambda_{calculated} = a\left(\frac{P}{65}\right)^b\left(\frac{T}{235}\right)^C \qquad \text{Equation D.4}$$

3. Calculate the total error

$$error = \sum_{i=1}^{n} \left(\lambda_{Aspen} - \lambda_{calculated}\right)_i^2 \qquad \text{Equation D.5}$$

4. Use Excel solver to minimize the total error to zero by changing the values of a,b and c.

Table D.1: Thermal Conductivity for *n*-Hexane using Aspen

T (K)	P (bar)	λ_{Aspen} (cal/cm.sec.K)	$\lambda_{calculated}$ (cal/cm.sec.K)	Error
313.15	0.68	2.76E-04	1.51E-08	7.64E-08
313.30	0.68	2.76E-04	1.52E-08	7.63E-08
327.31	1.13	2.65E-04	4.30E-08	7.00E-08
342.42	1.86	2.52E-04	1.19E-07	6.34E-08
367.09	3.81	2.31E-04	5.12E-07	5.32E-08
393.71	7.45	2.09E-04	2.01E-06	4.28E-08
421.25	13.67	1.86E-04	6.95E-06	3.20E-08
448.14	23.19	1.64E-04	2.04E-05	2.05E-08
472.52	35.81	1.43E-04	4.97E-05	8.75E-09
492.65	49.78	1.27E-04	9.75E-05	8.42E-10
506.87	61.67	1.14E-04	1.51E-04	1.34E-09
512.53	66.49	1.13E-04	1.76E-04	3.98E-09
511.14	65.53	1.14E-04	1.71E-04	3.31E-09
507.18	61.95	1.14E-04	1.53E-04	1.47E-09
504.36	59.47	1.17E-04	1.40E-04	5.58E-10
501.05	56.62	1.19E-04	1.27E-04	5.52E-11
495.29	51.87	1.24E-04	1.06E-04	3.33E-10
488.67	46.75	1.30E-04	8.57E-05	1.95E-09
481.28	41.47	1.36E-04	6.71E-05	4.75E-09
473.19	36.23	1.43E-04	5.09E-05	8.43E-09
459.96	28.77	1.54E-04	3.18E-05	1.49E-08
438.22	19.21	1.72E-04	1.39E-05	2.49E-08
415.19	12.04	1.91E-04	5.36E-06	3.44E-08
391.98	7.15	2.10E-04	1.85E-06	4.35E-08

358.72	3.02	2.38E-04	3.19E-07	5.66E-08
328.88	1.19	2.63E-04	4.80E-08	6.93E-08
315.45	0.74	2.75E-04	1.80E-08	7.54E-08
303.00	0.45	2.85E-04	6.63E-09	8.12E-08
291.47	0.27	2.95E-04	2.41E-09	8.67E-08
280.81	0.17	3.03E-04	8.70E-10	9.20E-08
266.29	0.08	3.15E-04	1.86E-10	9.95E-08
247.32	0.02	3.31E-04	1.80E-11	1.10E-07
Total				**1.26E-06**

The following Table D.2 shows the results obtained from linear regression.

Table D.2: Constants obtained by linear regression

a	0.000142
b	2.017551
c	0.218024

D.3. Thermal Conductivity of *Gas Phase Reaction*

The following Table D.3 shows the critical parameter used for gas-phase thermal conductivity calculation:

Table D.3: The critical parameter for Syngas

Component	Tc (K)	Pc (bar)	Zc	Vc (cm^3/mol)
H_2	32.98	12.93	0.303	64.2
CO	132.85	34.94	0.292	93.1
N_2	126.2	33.98	0.289	90.1

The thermal conductivity of the pure component was estimated using the relation of the thermal conductivity as a function of temperature at 1 bar as the following:

$$\lambda = A + BT + CT^2 + DT^3 \quad \text{Equation D.6}$$

where λ in W/m.K and T in K.

The thermal conductivities for H_2, CO and N_2 were calculated as the following at T=513 K.

Table D.4: Thermal conductivity calculation for gas-phase reaction

Component	A	B	C	D	lamda (W/m.K)	lamda (W/cm.K)	lamda (cal/cm.s.K)
H_2	8.01E-03	6.69E-04	-4.16E-07	1.56E-10	2.63E-01	2.63E-03	6.28E-04
CO	5.07E-04	9.13E-05	-3.52E-08	8.20E-12	3.92E-02	3.92E-04	9.36E-05
N_2	3.92E-04	9.82E-05	-5.07E-08	1.50E-11	3.94E-02	3.94E-04	9.43E-05

Then the thermal conductivity of the first component (syngas) was estimated as the following:

Table D.5: Thermal conductivity calculation for the syngas

Component	lamda (W/m.K)	yi (comp.)
H_2	2.63E-01	0.33
CO	3.92E-02	0.67

$$\lambda_1^o = \sum_{i=1}^{n} y_i \lambda_i = y_{CO}\lambda_{CO} + y_{H_2}\lambda_{H_2}$$

$$\lambda_1^o = (0.67)(2.63 \times 10^{-1}) + (0.33)(3.92 \times 10^{-2}) = 1.88 \times 10^{-1}\ W/m.K$$

$$\lambda_2^o = 3.94 \times 10^{-2}\ W/m.K$$

Calculation of the critical parameter for syngas mixture:

$$T_{C1} = \sum_{i=1}^{n} y_i T_{Ci} = y_{CO}T_{C-CO} + y_{H_2}T_{C-H_2}$$

$$T_{C1} = (0.67)(32.98) + (0.33)(132.85) = 66.27K$$

$$P_{C1} = \sum_{i=1}^{n} y_i P_{Ci} = y_{CO}P_{C-CO} + y_{H_2}P_{C-H_2}$$

$$P_{C1} = (0.67)(12.93) + (0.33)(34.94) = 20.27\ bar$$

$$Z_{C1} = \sum_{i=1}^{n} y_i Z_{Ci} = y_{CO}Z_{C-CO} + y_{H_2}Z_{C-H_2}$$

$$Z_{C1} = (0.67)(0.292) + (0.33)(0.303) = 0.3$$

$$V_{C1} = \frac{Z_{C1}\, R\, T_{C1}}{P_{C1}}$$

$$V_{C1} = \frac{(0.3)\ (83.15)\ (66.27)}{(20.27)} = 81.38\ cm^3/mol$$

$$M_1 = \sum_{i=1}^{n} y_i M_i = y_{CO} M_{CO} + y_{H_2} M_{H_2}$$

$$M_1 = (0.67)(2) + (0.33)(28) = 10.67 g/mol$$

$$\Gamma = \left(\frac{T_{C1} M_1^3}{P_{C1}^4}\right)^{1/6}$$

where Γ is in m.K/W, T_{C1} is in K, M is in g/mol and P_{C1} is in bar.

$$\Gamma_1 = \left(\frac{(66.27)(10.67)^3}{(20.27)^4}\right)^{\frac{1}{6}} = 0.8839\ m.K/W$$

$$\Gamma_2 = \left(\frac{(66.27)(126.2)^3}{(33.98)^4}\right)^{\frac{1}{6}} = 1.1296\ m.K/W$$

To account for the influence of pressure, since the operating pressure is 80 bar, the following correction was used:

Table D.6: Compressibility factor for the syngas

Component	Z
H_2	1.04
CO	1.025

$$Z_1 = (0.67)(1.04) + (0.33)(1.025) = 1.035$$

$$Z_2 = 1.025$$

$$V_{C1} = \frac{(1.035)\ (83.15)\ (513)}{(80)} = 551.83\ cm^3/mol$$

$$V_{C1} = \frac{(1.025)\ (83.15)\ (513)}{(80)} = 546.50\ cm^3/mol$$

$$\rho_{r1} = {}^{V_{C1}}/_{V_1} = 88.67/551.83 = 0.15$$

$$\rho_{r1} = {}^{V_{C1}}/_{V_1} = 88.67/546.50\ = 0.15$$

Then,

$$(\lambda_{m1} - \lambda_m^{\circ}) = 1.22 \times 10^{-2}\left[\exp\left(0.535(0.15)\right) - 1\right]/[(0.8839)(1.035)^5]$$

$$= 9.54 \times 10^{-4}$$

$$(\lambda_{m2} - \lambda_m^{\circ}) = 1.22 \times 10^{-2}\left[\exp\left(0.535(0.15)\right) - 1\right]/[(1.1296\ )(1.025)^5]$$

$$=\ 7.92 \times 10^{-4}$$

$$\lambda_{m1} = 9.54 \times 10^{-4} + 1.88 \times 10^{-1} = 1.89 \times 10^{-1}$$

$$\lambda_{m2} =\ 7.92 \times 10^{-4} + 3.94 \times 10^{-2} = 4.02 \times 10^{-2}$$

Then,

$$k_{mL} = \lambda_{m1}\left(y_{H_2} + y_{CO}\right) + \lambda_{m2}\, y_{N_2} = 1.89 \times 10^{-1}(0.17 + 0.08) + 4.02 \times 10^{-2}(0.75)$$

$$= 7.75 \times 10^{-2}\ W/m.K$$

$$k_{mR} = \frac{1}{\left(y_{H_2} + y_{CO}\right)/\lambda_{m1} + \ y_{N_2}/\lambda_{m2}}$$

$$= \frac{1}{(0.17 + 0.08)/1.89 \times 10^{-1} + (0.75)/4.02 \times 10^{-2}}$$

$$= 5.01 \times 10^{-2}\ W/m.K$$

$$k_m = (1 - q)k_{mL} + qk_{mR} = (1 - 0.54)7.75 \times 10^{-2} + (0.54)5.01 \times 10^{-2}$$

$$= 6.27 \times 10^{-2}\ W/m.K$$

APPENDIX E

FUGACITY BASED MACRO-SCALE MASS BALANCE

The mass balance equation of fixed-bed reactor, packed with solid catalyst particle is given by the following equation:

$$F_i = F_i + dF_i + \eta_o \rho_B (-v_i) r dV \quad \text{Equation E.1}$$

where F_i is the molar flow rate of species i, η_o is the overall effectiveness factor, ρ_B is the bed density (mass of catalyst/ volume of bed), v_i is the stoichiometric coefficient of species i, r is the rate of reaction over the solid catalyst (mole/mass of catalyst/time).

Since $F_i = uA_C C_i \; and \; V = A_C z$, the previous equation gives the following assuming that u and A_C are not a function of z:

$$-u \frac{dC_i}{dz} = \eta_o \rho_B (-v_i) r \quad \text{Equation E.2}$$

where u is the superficial velocity and C_i is the concentration of species i.

Equation E.1 is obtained in terms of fugacity by utilizing the real gas low as follows:

$$PV = znRT \quad \text{Equation E.3}$$

$$P = zCRT \text{ , } where \; C = \frac{n}{V}$$

$P_i = zC_i RT$ (For multicomponent system)

$$C_i = \frac{P_i}{zRT}$$

$$f_i = y_i P \Phi_i = P_i \Phi_i \quad \text{Equation E.4}$$

$$Then, \; C_i = \frac{f_i}{z \Phi_i RT}$$

$$\frac{d\left(\frac{u_s f_i}{z\Phi_i RT}\right)}{dZ} = -\eta_o \rho_B (-v_i) r \qquad \text{Equation E.5}$$

Applying the chain rule on the previous equation E.5 gives:

$$\frac{u_s}{z\Phi_i RT}\frac{df_i}{dZ} + \frac{f_i}{z\Phi_i RT}\frac{du_s}{dZ} - \frac{u_s f_i}{z\Phi_i RT^2}\frac{dT}{dZ} = -\eta_o \rho_B (-v_i) r$$

By assuming no change of u_s, z and Φ_i in the axial direction, the partial pressure dependency of Z:

$$\frac{u_s}{z\Phi_i RT}\frac{df_i}{dZ} - \frac{u_s f_i}{z\Phi_i RT^2}\frac{dT}{dZ} = -\eta_o \rho_B (-v_i) r \qquad \text{Equation E.6}$$

Rearranging Equation E.6 gives the following expression:

$$\frac{df_i}{dZ} - \frac{f_i}{T}\frac{dT}{dZ} = -\frac{z\Phi_i\, R\, T\, \eta_o \rho_B (-v_i) r}{u_s} \qquad \text{Equation E.7}$$

APPENDIX F

OVERALL HEAT TRANSFER COEFFICIENT CALCULATION

$$\frac{1}{U} = \frac{1}{\alpha_i} + \frac{d}{\lambda_{wall}}\frac{A_b}{A_m} + \frac{1}{\alpha_u}\frac{A_b}{A_u} \quad \text{Equation F.1}$$

$$\alpha_i = \alpha_i^0 + 0.033\frac{\lambda_g}{d_p}\mathrm{Pr}_g\mathrm{Re}_g \quad \text{Equation F.2}$$

$$\alpha_i^0 = \frac{10.21\lambda_e^0}{{d_t}^{4/3}} \quad \text{Equation F.3}$$

A_b, A_u and A_m are given by the Equation F.4 and Equation F.5 respectively.

$$A_b = \pi d_t L \quad \text{Equation F.4}$$

$$A_u = \pi(d_t + d)L \quad \text{Equation F.5}$$

$$A_u = \frac{(A_u - A_b)}{\log\left(\frac{A_u}{A_b}\right)} \quad \text{Equation F.6}$$

The thermal conductivity of the wall is $20\,W/m.K$ assuming that the reactor wall is made of the stainless steel. The heat transfer coefficient for the medium side is $50\,W/m^2.K$ assuming that the reactor tube is surrounded by air. The thermal conductivity of the solid catalyst particles and the fluid is given by the previously mentioned Equation 4.12 and 4.14, respectively. The physical properties used to calculate Re and Pr numbers were calculated using Aspen as per the following Table F.1.

Table F.1: Physical properties from Aspen at T=513K and P=80 bar

Specific heat capacity of *n*-Hexane, C_P	3.73E03 KJ/kg.K
Viscosity of *n*-Hexane, μ	5.30E-05 kg/m.s
Specific heat capacity of syngas and N_2, C_P	1.31 KJ/kg.K
Viscosity of syngas and N_2, μ	2.60E-05 kg/m.s

APPENDIX G

NUMERICAL SOLUTION USING MATLAB

G.1. Micro-Scale Modeling for SCF- FTS

```
function ex6bvp2
This code shows how to deal with a singular
%   coefficient arising from reduction of a partial differential
equation to
%   an ODE by symmetry.  Also, for the physical parameters considered
here,
%   the problem has three solutions.
  % y(1) = fCO
  % y(2) = y(1)'
  % y(3) = T
  % y(4) = y(3)'
  % y(5)=fH2
  % y(6)=y(5)'

%% Operating Conditions
  x=0;
  Tb=513;%Operating Temp. in K
  Pb=65; %Operating Pressure in bar
  s=3;% Hexane to Syngas feed ratio
  v=2;%H2 to CO feed ratio
  alpha=0.85; % ASF chain growth probability

%%  Define the physical parameters for this problem.

%RohCat=1.5; %Catalyst density in g/cm3
RohCat=1.159; %Catalyst density in g/cm3
Vp=0.42; %Pellet pore volume in cm3/g
%DCOe=1.5e-4;  % effective diffusivity of CO in SCH in cm2/s
%DH2e=5.71e-4; % effective diffusivity of H2 in SCH in cm2/s
R=83.14; % Universal gas constant in bar.cm3/mol.K
dp=1; %catalyst diameter im mm
Rp=(dp/2)*100/1000; % Is the pellet radius in Cm
dH = -146e3; %-43021; %Heat of reaction (J/mol)
ep = RohCat*Vp; % porosity of the pellet (assumed)
%ep=0.5;
t=3.5; % pellet tortuosity (assumed)

% Parameter for Diffusivity calculation
M1=86.18; % is the molecular W for Hexane in kg/kmol
VC1=371; % is the critical molar V in cc/mol
PC1=30.25; % Critical pressure in bar
V=209.34; %403.25; % the molar V of hexane at T=513 and P=80 bar (from
aspen using SRK EOS)
K1=1;
M2CO=28; % is the molecular W for CO in Kg/kmol
```

```
M2H2=2; % is the molecular W for H2 in Kg/kmol
VC2CO=94.4; % is the molar v of CO in cc/mol
VC2H2=64.15; % is the molar v of H2 in cc/mol
d=dp*10^7; % is the pore dimater in A

[fug,Vm,Mm,Y,Z,phi,r] = hexane_selectivity(Tb,Pb,x,s,v);

%[fug,Vm,Mm,Y,Z,phi,r] = inlet_fugacities(Tb,Pb,s,v,'Hexane');


phiCO=phi(1);
phiH2=phi(2);
fugCO=fug(1);
fugH2=fug(2);

guess_f  = 0.5;
guess_T  = Tb;
guess_fH2  = 0.5;

  solinit = bvpinit(linspace(0,1,100),[guess_f 0 guess_T 0 guess_fH2
0]);
  sol = bvp4c(@ex6ode,@ex6bc,solinit);


%The Main Result

x = real(sol.x)'; % dimensionless radius r/Rp
y1 = real(sol.y(1,:))'; % dimensionless CO fugacity fCO/fCOb
fCO = y1.*fugCO;
y5= real(sol.y(5,:))';
fH2=y5.*fugH2;
y2 = fH2./fugH2; % dimensionless H2 fugacity fH2/fCOb
y3 = real(sol.y(3,:))'; % temperature, in K
r = x.*Rp; % radius in cm
% Conversion calculation
xCO = (fugCO - min(fCO))/fugCO; % conversion

% Effective diffusivity calculation in cm2/s
DCOe=(((0.61614+(3.0902*exp(-0.87756*((sqrt(M1*VC1))/PC1))))*(((V^K1)-
23)*10^-6)*(sqrt(y3/M2CO)))*ep/t)*((1-(0.841*(VC2CO^0.333)/d))^4);
DH2e=(((0.61614+(3.0902*exp(-0.87756*((sqrt(M1*VC1))/PC1))))*(((V^K1)-
23)*10^-6)*(sqrt(y3/M2H2)))*ep/t)*((1-(0.841*(VC2H2^0.333)/d))^4);

% Effectivness factor calculation

k=kCO(1)*exp((-Ea(1)/R)*((1/y3)-(1/Tb)));
k1=kCO(2)*exp((-Ea(2)/R)*((1/y3)-(1/Tb)));
k2=kCO(3)*exp((-Ea(3)/R)*((1/y3)-(1/Tb)));
k3=kCO(4)*exp((-Ea(4)/R)*((1/y3)-(1/Tb)));
```

```
Rco=
(k*(fCO.^0.5).*(fH2.^0.5))/((1+k1*fH2.^0.5+(k2*fCO.^0.5)+k3*(fCO)).^2)/
60;
eta_numerical= (3*trapz(r,(Rco.*(r.^2))))/((Rp^3)*max(Rco))

Data=[ x y1 y5]

%% Thiele Modulus Calculation
L= (Rp/100)/3; % is the characteristic length for Sphere in m
h=287.4953; %Convective heat transfer W/m2.K (Detailed calculation in
Excel)
DTfilm=real(-dH*(max(Rco)*(100^3)*RohCat)*L/h) % the rate of reaction
in the unit mol/m3.S To know is the External heat transfer is important
or not
Ts=Tb+DTfilm; % Ts in K
kg=4.30E-04; % Convective mass transfer coef. in m/s
CCOg= max(fCO)*(100^3)/(R*Tb); % the concentration in mol/m3
ratio=((max(Rco)*(100^3)*RohCat)*L)/(kg*CCOg);% To know if the External
Mass transfer is important of not
CCOs=CCOg*(Tb/Ts);
DCOe=(((0.61614+(3.0902*exp(-0.87756*((sqrt(M1*VC1))/PC1))))*(((V^K1)-
23)*10^-6)*(sqrt(Tb/M2CO)))*ep/t)*((1-(0.841*(VC2CO^0.333)/d))^4); % In
Cm2/s
Mw=real(((max(Rco)*(100^3)*RohCat)*(L^2))/((DCOe/(100)^2)*CCOs)) % TO
know if the internal MT or pore diffusion is important
ks = (0.8652+0.00108*(Tb-273.15))/100; %thermal conductivity of the
solid in W/cm.K (J Thermophys., 2010, 31:556-571)
kf = 0.0005941*(Pb/65)^2.0176*(Tb/235)^0.218; %thermal conductivity of
the sc. hexane  in W/cm.K (from Aspen)
ke=(ks*((kf/ks)^ep))*100; % the effective thermal conductivity in W/m.K
beta=real((DCOe/(100)^2)*(-dH)*CCOs/(Ts*ke))
Thiele=real(sqrt(Mw/eta_numerical))

if Mw>4
    eta_calculated=1/Mw
elseif Mw<0.15
    eta_calculated=1
else error('Read eta from the graph');
end

%% Plot data in one Figure
 % use the subplot (m,n,nr

m=2; % m=2 because I have two plots fCO/fCOb and fH2/fCOb Vs r/Rp
n=1;
nr=1; % to be in the upper window
subplot(m,n,nr);
plot(x,y1),hold on, plot(x,y2,'-r');
      axis([0 1 -0.1 1.1])
      title('Dimensionless Fugacity Profiles')
      xlabel('\itr\rm / \itR\rm_p')
      ylabel('\itf\rm / \itf\rm_[8]')
      legend('CO','H_2','location','NorthWest');
```

```
% To plot the Tempreture Profile
nr=nr+1; % to be in the lower window
subplot(m,n,nr);
plot(x,y3)
      title('Temperature Profile')
      xlabel('\itr\rm / \itR\rm_p')
      ylabel('T / K')


% ------------------------------------------------------------------
-----
%% Rate Expression



function dydx = ex6ode(x,y)
%EX6ODE  ODE function for Example 6 of the BVP tutorial.

dydx = [y(2); 0; y(4); 0; y(6); 0];
% Rate Expression
kCO = [4e-4 0.169 0.2 2e-4]; % Arhenius constants [k k1 k2 k3] Units
are mol/gcat.min.bar
Ea = [-1.25e4 6.026e3 -1.798e4 8.997e3]; % (Ea/R) from diffusion paper
R is 8.314 J/mol.K
T=y(3); % Remove this after adding the heat equation
k=kCO(1)*exp((-Ea(1)/R)*((1/T)-(1/Tb)));
k1=kCO(2)*exp((-Ea(2)/R)*((1/T)-(1/Tb)));
k2=kCO(3)*exp((-Ea(3)/R)*((1/T)-(1/Tb)));
k3=kCO(4)*exp((-Ea(4)/R)*((1/T)-(1/Tb)));


rCO= (k*((y(1)*fugCO)^0.5)*((y(5)*fugH2)^0.5))...

/((1+k1*((y(5))*fugH2)^0.5+(k2*(y(1)*fugCO)^0.5)+k3*(y(1)*fugCO))^2)/60
;
% The unit of rCO is % mol/gcat.s ( Multiply by fCOb in the rate
equation to have rCO in the dimentionless form)

DCOe=(((0.61614+(3.0902*exp(-0.87756*((sqrt(M1*VC1))/PC1))))*(((V^K1)-
23)*10^-6)*(sqrt(y(3)/M2CO)))*ep/t)*((1-(0.841*(VC2CO^0.333)/d))^4);
%the effective diffusivity of CO in cm2/s
DH2e=(((0.61614+(3.0902*exp(-0.87756*((sqrt(M1*VC1))/PC1))))*(((V^K1)-
23)*10^-6)*(sqrt(y(3)/M2H2)))*ep/t)*((1-
(0.841*(VC2H2^0.333)/d))^4);%the effective diffusivity of H2 in cm2/s


temp_fCO=(R*(y(3))*Rp^2/(DCOe*fugCO))*(rCO)*RohCat*phiCO*Z; % This term
for mass balance equation for CO
```

```
temp_fH2=((R*(y(3))*Rp^2/(DH2e*fugH2))*(rCO)*RohCat)*(3-alpha)*phiH2*Z;
% This term for mass balance equation for H2

% This part for heat equation
ks = (0.8652+0.00108*(y(3)-273.15))/100; %thermal conductivity of the
solid in W/cm.K (J Thermophys., 2010, 31:556-571)
kf = 0.0005941*(Pb/65)^2.0176*(y(3)/235)^0.218; %thermal conductivity
of the sc. hexane  in W/cm.K (from Aspen)
%kf=4.058e-4; %thermal conductivity of the sc. hexane  in W/cm.K
Calculated using Dr. Bukur notes and the book the properties of gases
and liquids at T=513K and P=80 bar
lambda=ks.*((kf./ks).^ep); % This is the effective thermal conductivity
in W/cm.K

temp_T = ((dH*RohCat*Rp^2)/(lambda))*(rCO);


if x == 0
  dydx(2) = (1/3)*temp_fCO;
  dydx(4) = (1/3)*temp_T;
  dydx(6) = (1/3)*temp_fH2;


else
  dydx(2) = -(2/x)*y(2) + temp_fCO; % the full mass balance equation
  dydx(4) = -(2/x)*y(4) + temp_T;
  dydx(6) = -(2/x)*y(6) + temp_fH2; % the full mass balance equation

end

end
% ------------------------------------------------------------------------
-----

function res = ex6bc(ya,yb)
%EX6BC  Boundary conditions for Example 6 of the BVP tutorial.
res = [ ya(2)
        ya(4)
        ya(6)
        yb(1) - 1
        yb(3) - Tb
        yb(5) - 1];
end

end
```

G.3. Macro-Scale Modeling for SCF-FTS

```
function dydz = f(z,y)

global fCOinlet zend alpha ;
y = real(y);

%% Operating Condition
Tr= 513; % T in K
Pr=80; % total pressure in bar
s=3;% Hexane to Syngas feed ratio
v=2;%H2 to CO feed ratio
x = (fCOinlet - y(2)) / fCOinlet; % conversion

% Constants
dH=146; % kJ/mol, heat of reaction
Cp=3.73E-03;  % specific heat capacity of hexane in [KJ/g.K]
R=83.14; % Universal gas constant in [bar*cm3/mol*K]

% calculation of the density of the gas rohg

[fug,Vm,Mm,Y,Z,phi,r] = hexane_selectivity(y(1),y(3),x,s,v); %evaluate
molar vol and molar mass of mixture using a mod SRK EoS
y(2) = fug(1); % new CO fugacity
rhog = Mm*1000/Vm; % g/cm3, fluid density
eta= ex6bvp2(Tr,Pr, fug, Z, phi);

%% The calculation of Us
dt =1.75; % is the tube diameter[cm]
Qinlet=150; % The total inlet flow rate at standard conditions in
cm3/min
yCO=1/3;
QCOinlet = Qinlet*yCO/60; % ml/s In this case I triple the flow rate Q
total=150
Ps = 1; % standard pressure in bar
Ts = 293.15; % standard temperature in K
molCOinlet = (Ps*QCOinlet)/(R*Ts); % mol/s, using Ideal Gas Law
molCO = (1-x)*molCOinlet; % number of moles of CO at a given conversion
moltot = sum((Y./Y(2))*molCO); % total number of moles in mixture
Q = Vm*moltot; % cm3/s, vol. flowrate of mixture
At=pi*((dt/2)^2);% tube cross section in [cm2]
supvel = Q/At; % superficial velocity, cm/s

%% The calculation of U
Z=zend; % length of catalyst bed in [cm]
dxw = 0.7925; % cm, wall thickness ( detailed calculation is available
in the excel sheet)
dp = 0.1; % particle diameter in [cm]
ep=0.5; %bed porosity
mtot = moltot*Mm; %  mass flowrate of mixture in kg/s
Gg = mtot*1000*(100^2)/At; % kg/m2.s, mass flux into reactor
```

```
mu_g=5.36E-02; %SC hexane viscosity at 80 bar and 513 K using ASPEN in
[g/m*s]
Cp2 = 0.32115; % specific heat capacity of hexane in [kJ/mol.K]
lambda_g = 0.05941*(y(3)/65)^2.0176*((y(1)-273.15)/235)^0.218/1000; %
kW/m.K, fluid-phase thermal conductivity (ASPEN data, Aswani)
lambda_wall = 20/1000; % wall thermal conductivity for Stainless Steel
in [kW/m.K]
alpha_u = 50/1000; %air-side htc (assuming tube surrounded by air) in
[kW/m2.K]
Ab = pi*dt*Z; % bed side area in [cm2]
Au = pi*(dt+dxw)*Z; %  outer fluid side area in [cm2]
Am = (Au-Ab) / log(Au/Ab); % log mean area in [cm2]
Re_g = Gg*(dp/100)/mu_g/(1-ep); % Reynolds number for packed bed
Pr_g = Cp2*mu_g/lambda_g/Mm; % Prandtl number
alpha_i = lambda_g/(dp/100)*0.033*Pr_g*Re_g; % De Wasch and Froment
(1972), assuming static contribution is zero
U = (10*(1/alpha_i + (dxw/100)/lambda_wall*Ab/Am + 1/alpha_u*Ab/Au)^-
1)/(100^2); % overall htc, kW/cm2.K

%% To Calculate the bed density
ep=0.5; %bed porosity
RohCat=1.5; %Catalyst density in g/cm3
rhob=RohCat*(1-ep); % Bed density  in g/cm3

%% Rate of reaction
kCO = [4e-4 0.169 0.2 1e-4]; % Arhenius constants [k k1 k2 k3] Units
are mol/gcat.min.bar
Ea = [-1.25e4 6.026e3 -1.798e4 8.997e3]; %exponential contants (= Ea/R)
from Aswani's diffusion paper
k=kCO(1)*exp((-Ea(1)/R)*((1/y(1))-(1/Tr)));
k1=kCO(2)*exp((-Ea(2)/R)*((1/y(1))-(1/Tr)));
k2=kCO(3)*exp((-Ea(3)/R)*((1/y(1))-(1/Tr)));
k3=kCO(4)*exp((-Ea(4)/R)*((1/y(1))-(1/Tr)));
fH2 = (3-alpha)*y(2); % from reaction stoichiometry, Aswani's diffusion
paper

rCO= (k*((y(2))^0.5)*((fH2)^0.5))...
            /((1+k1*(fH2)^0.5+(k2*(y(2))^0.5)+k3*(y(2)))^2)/(60); % The
unit of rCO is % mol/gcat.s
%% Friction factor
f = 6.8*(1-ep)^1.2/ep^3*Re_g^-0.2; % Hicks (1970) from Froment p.509 -
for packed bed of spheres

%% ODE system
dydz= zeros(3,1);
dydz(1)=1.0/(supvel*rhog*Cp)*(dH*rhob*rCO-4.0*U/dt*(y(1)-Tr)); % Heat
balance equation
dydz(2)=((-phi(1)*eta*rhob*R*y(1)*rCO)/supvel)+(y(2)*dydz(1))/y(1); %
Mass balance equation
dydz(3)=-(f*rhog*supvel^2*1e-4/dp)*1e-5 ; % Pressure drop

end
```

```
clear all

global fCOinlet zend alpha;

%% Operating Condition to calculate the initial fugacity
Tr= 513; % T in K
Pr=80; % total pressure in bar
s=3;% Hexane to Syngas feed ratio
v=2;%H2 to CO feed ratio
alpha=0.85; % ASF chain growth probability

[fug,Vm,Mm,Y,Z,phi,r] = inlet_fugacities(Tr,Pr,s,v,'Hexane');

%% The integration interval over which Matlab should integrate.
zstart = 0; % cm, inlet zone
zend = 5; % cm, outlet zone
zspan=[zstart zend];

% The initial values can be put into a vector called y0.
fCOinlet=fug(1); %[bar]
T0 = 513; %[K]
P0=80; %[bar]
y0=[T0 fCOinlet P0];

[z,y]=ode45('f',zspan,y0);


%% To plot the resuts, I use the subplot (m,n,nr)
m=2; % m=2 because I have two plots fCO and T Vs Z
n=1;
nr=1; % to be in the upper window
subplot(m,n,nr);
plot(z,real(y(:,1)))
title('Temperature profile')
xlabel('z [cm]')
ylabel('T [K]')
nr=nr+1; % to be in the lower window

xCO = (fCOinlet - real(y(:,2))) / fCOinlet;
fH2 = (3-alpha)*real(y(:,2));
subplot(m,n,nr);
plot(z,xCO)
title('Conversion')
xlabel('z [cm]')
ylabel('XCO')
data=[ real(y(:,1)) real(y(:,2)) xCO z fH2 real(y(:,3))];
```